Analysing the effects of earthquakes on wind turbines

Oliver Claxton

Thesis of 30 ECTS credits
Master of Science in Civil Engineering with specialization in Structural Design

June 2014

Analysing the effects ofearthquakes on wind turbines

Oliver Claxton

Thesis of 30 ECTS credits submitted to the School of Science and Engineering
at Reykjavík University in partial fulfillment
of the requirements for the degree of
Master of Science in Civil Engineering
with specialization in Structural Design

June 2014

Supervisor(s):

Jónas Þór Snæbjörnsson
Professor, Reykjavík University, Iceland.

Examiner(s):

Ragnar Sigbjörnsson
Professor, University of Iceland, Iceland

Abstract

Modern wind parks are largely built in areas where seismic risk is low. With an increased emphasis on the use of wind power it may be assumed that wind turbines will in the future increasingly be built in areas where higher seismic risk exists. The aim of this study is to gain insight into the importance of earthquake action for wind power installations as well as attain improved understanding of the dynamic behaviour of wind turbine structures. Wind turbines are special type of structures as they are slender but with a large top-mass. On one hand their slenderness and relatively long first natural period may reduce the seismic effects, but on the other hand the high top-mass will increase the earthquake induced inertia force. This study uses recorded acceleration data from three large Icelandic earthquakes to evaluate the seismic response of a typical wind turbine assuming that it is located at the recording site. A 0.9 MW Enercon wind turbine recently erected near the Búrfell Power Station in South Iceland is used as for the case study. The turbine is modelled using FEM technique in SAP2000 and Matlab. The analysis workflow includes the selection of seismic data, modal analysis, response history analysis and response spectrum analysis. Through these analyses an estimate of potential seismic vulnerability of wind turbines in an Icelandic environment is achieved. Key response parameters, such as the top displacement, base shear and base moment are systematically evaluated using both time history analysis and response spectrum analysis. The methods applied are in line with analysis methods recommended by the various relevant design guidelines. Their systematic application gives insight into their applicability and may, among other things, provide supportive information for designers regarding the appropriate methodology for assessing the influence of earthquakes on wind turbines.

Ágrip

Nútíma vindorkuver eru að mestu byggð á svæðum þar sem jarðskjálfta hætta er lítil . Með aukinni áherslu á notkun vindorku má gera ráð fyrir að vindorkuver verði í framtíðinni í auknu mæli byggð á svæðum þar sem jarðskjálftahætta er til til staðar. Markmið þessarar rannsóknar er að fá innsýn í mikilvægi jarðskjálfta fyrir vindorkumannvirki og öðlast betri skilning á sveiflufræðilegri hegðun vindurtúrbína. Hefðbundnar vindtúrbínur sem snúast um láréttan ás, eru sérstök tegund mannvirkja þar sem vindhverfillinn hvílir á háum sveigjanlegum turni. Stífni virkisins er því tiltölulega lítil en meirihluti massans er staðsettur í toppi turnsins. Þessir eiginleikar, það er tiltölulega langur fyrsti eiginsveiflutími, geta dregið úr áhrifum jarðskjálfta á mannvirkið en á hinn bóginn veldur mikill massi efst í virkinu verulegum massatregðukröftum sem geta aukið jarðskjálftaálagið. Þessi rannsókn notar skráð hröðunargögn úr þremur stórum íslensku jarðskjálftum til að meta jarðskjálftasvörun dæmigerðrar vindtúrbínu. Miðað er við að vindtúrbínan sé staðsett á sömu stöðum og hröðunarmælingarnar fóru fram. Útreikningarnir miðast við 0,9 MW Enercon vindtúrbínu sem nýlega var reist nálægt Búrfellsvirkju inn á suðurhálendi Íslands. Byggt er líkan af turninum með einingaraðferðinni í SAP2000 og Matlab. Greiningarferlið felur í sér innlestur jarðskjálftagagna, uppbyggingu kerfisfylkja, eiginsveiflugreiningu og svörunargreiningu. Markmiðið er að fá fram mynd af jarðskjálftaáhrifum og jarðskjálftasvörun vindtúrbina sem eru staðsettar í mismunandi fjarlægð frá upptökum stórra jarðskjálfta. Farið er kerfisbundið í gegnum allar mældar grunnhröðunarraðir úr þeim þrem jarðskjálftum sem birtar hafa verið í ISESD gagnagrunninum. Birtar eru lykil svörunarstærðir, svo sem færslur, skúfkraftar og vægi. Bæði er beitt tímaraðargreiningu og svörunarrófsgreiningu. Notaðar eru þær greiningaraðferðir sem helstu hönnunarstaðalar og leiðbeiningar mæla með. Kerfisbundin beiting þeirra gefur innsýn í notagildi þeirra sem meðal annars getur nýst hönnuðum við val á viðeigandi aðferðum til að meta áhrif jarðskjálfta á vindtúrbínur.

Analysing the effects of earthquakes on wind turbines

Oliver Claxton

30 ECTS thesis submitted to the School of Science and Engineering at
Reykjavík University in partial fulfillment of
the requirements for the degree of
Master of Science in Civil Engineering
with specialization in Structural Design

June 2014

Student:

_____

Oliver Claxton

Supervisor(s):

_____

Jónas Þór Snæbjörnsson

Examiner:

_____

Ragnar Sigbjörnsson

Preface

In the past few years more and more emphasize has been put on renewable energy. One of the useable options for renewable energy is wind energy through wind turbines. Wind turbine farms have been established over the whole world and even though xx% of energy use in Iceland is renewable energy the idea of wind turbines in Iceland has become louder and louder. Icelandic authorities are even looking into the option of putting up wind farm. One of the factors that need to be considered for the design of wind turbines in Iceland is seismic activity and the effect of earthquakes on the structure of wind turbines. Through my studies I have gained interest in structural design and the effects of seismic activity on structures. The idea for this thesis came from my supervisor, Jónas Þór Snæbjörnsson, who pointed out that not much attention had been given towards the effects of earthquakes on wind turbines. Few studies have been done to cast a light on this subject and guidelines have been generated, *Guidelines for Design of Wind Turbines* (Risø, 2001), *Guideline for the Certification of Wind Turbines* (GL, 2003) *and IEC 61400-1 Ed.3: Wind turbines - Part 1: Design requirements* (IEC, 2005).

In this thesis I will test the effects of two large earthquakes the occurred in Iceland in 2000 and 2008 on specific types of wind turbines and use Matlab and SAP to xxxxx and compare that to previous research and tests that have been conducted on the effects of earthquakes on wind turbines.

Acknowledgement

First of all I would like to thank my supervisor, Jónas Þór Snæbjörnsson, for his support and guidance through this process and his valuable input. I would also like to thank my family, my soon to be wife, Svandís H. Halldórsdóttir for her input, support and reading of the thesis and my children, Hrönn and Dagur, for their patience as well has my parents and parents in-laws.

Contents

List of Figures

List of Tables

1 Introduction

1.1 Wind turbines and wind energy

1.1.1 History

Through the decades wind has been used to generate power for different reasons and through different methods, the first known usage of wind to power a machine can be traced back to the first century when the Greek engineer Heron of Alexandria created his wind wheel (James & Thorpe, 1994). Wind powered ships, grain mills, water pumps, and threshing machines are examples of ancient use of wind power machines that utilize the wind to execute mechanical tasks to ease labour. During the 20th century wind turbines, machines with rotating blades that convert the kinetic energy of wind into useful power, were developed (Risø, 2001). The first known use of wind turbines to generate power is from the late nineteenth century when Brush constructed a 12 kW DC windmill generator in the USA. However, during the early years of the 20th century wind turbines received very little interest until the price of oil rose dramatically in 1973 (Burton, Sharpe, Jenkins, & Bossanyi, 2001).

1.1.2 Wind energy

In 1973 a stimulus for the development of wind energy emerged due to the price of oil and concern over limited fossil-fuel resources. This later shifted towards CO_2 emission and the wind energy potential to help limit climate change. The Commission of the European Union called in 1997 for 12 percent of the gross energy demand to be contributed from renewables by increasing wind turbine capacity from 2.5 GW in 1995 to 40 GW by 2010 (Risø, 2001).

In 2012 wind energy production continues to grow rapidly with almost 45 GW of capacity built worldwide and a total production approaching 285 GW (Wiser & Bolinger, 2013). Due to this growth, recent installations are expanding into high seismic hazard regions, such as USA, China and now Iceland. Therefore regulating agencies have included seismic requirements for certifying wind turbines (Germanischer Lloyd, 2003), (IEC, 2005).

Icelandic authorities are looking at wind turbines as a third option in renewable energy when almost entire commercial electricity production in Iceland comes from green energy, i.e. 71,8% from hydropower, 24% from geothermal power, 4,1% from fossil-fuel and since 2013 0,1% from wind power (Orkustofnun, 2013). Wind turbines are believed to be an important source of low-impact renewable energy when used in combination with hydro-electric power, due to high wind speed and reduced stream flow and reduced sunlight during the winter time. Unlike solar energy, wind power can be used throughout the year, therefore reducing the need for water regulation.

In 2013 a research was conducted by the Icelandic Meteorological Office and the University of Iceland to determine the wind energy potential in Iceland. After preliminary research of suitable wind farm sites, 14 test sites were selected for more detailed analyses, 10 are located near the coast chosen for their accessibility and four inland near a hydro- and geothermal power plants, Figure 1-1. Out of these 14 sites two experimental 900 kW turbines have been erected next to Búrfell hydro-power plant, with expected energy capacity of 54 GWh per year. The specifications of these experimental turbines will be discussed further later in this paper.

According to the Meteorological Office research the energy potential of Iceland is not a limiting factor for wind energy production since it is within the highest class as defined in the European Wind Atlas. That would suggest that Iceland is a suitable placement for wind-power farms, however the report does not take into account the seismic activity in Iceland especially in South Iceland, it mainly states that seismic activity cannot be excluded (Nawri, et al., 2014).

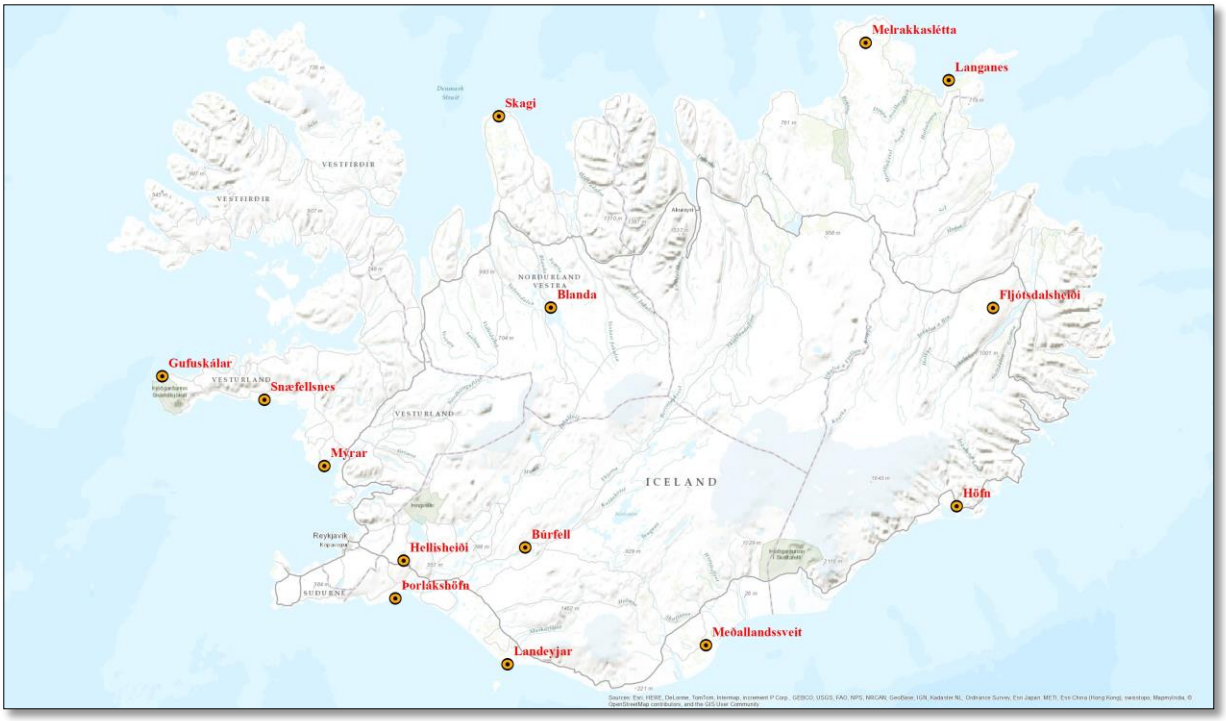

Figure 1-1. Topographic map of Iceland, showing the location of sites, for which detailed analyses of wind energy potential were performed, shown in orange.

1.1.3 Wind turbines

In the 20th century many wind turbine designs were developed, including horizontal axis and vertical axis turbines (Risø, 2001). The primary designs for the turbine tower were a truss and a tube tower. The truss tower was used by many designers as it is similar to other existing designs, i.e. electrical transmission towers. Others opted for the tube tower, made of steel and constructed by rolling flat steel plates to the desired diameter and welding to join. In the recent years designers have look towards the use of pre- or posttensioned concrete as an alternative construction material for the tube tower.

The most common wind turbines used for large scale electricity production today are classified as two or three bladed turbines with horizontal axes and upwind rotors. Horizontal axis wind turbine (HAWT) has three main components, a tower, a nacelle and a rotor. The turbine hub, connecting the three blades together, referred to as the rotor, is connected to the nacelle trough the drive shaft. Inside the nacelle the generator and gear box are placed among other mechanical components needed to support the rotor. The Tower supports the nacelle and rotor, elevating it to the desired height.

Figure 1-2 shows a glimpse into the nacelle of an Enercon wind turbine, similar to those in current operation by Landsvirkjun in the Burfell area.

This thesis focuses on three bladed, horizontal axis, active yaw, and upwind power generation wind turbines supported by tubular steel towers.

Figure 1-2. Rotor and Nacelle (Enercon)

1.2 Problem statement

Modern wind parks are largely built in areas where earthquakes are rare and/or have low impact. With the increased emphasis on the use of renewable energy, including wind power it can be assumed that wind turbines will increasingly be built in areas where higher seismic risk exists.

Presently two large test wind turbines have been constructed in Iceland and a wind power park is being planned. Iceland is a seismically active country, where earthquakes of up to magnitude 7 can be expected.

This study uses recorded acceleration data in three large Icelandic earthquakes to evaluate the seismic response of a typical wind turbine if located at the recording site. Through these analysis, an estimate of potential seismic vulnerability of wind turbines in an Icelandic environment is achieved.

Wind turbines differ from other regular structures, as they are slender structures with large a top-mass. On one hand their slenderness may reduce the seismic effects, but on the other hand the high top-mass will increase the earthquake induced inertia force.

The research questions this study is meant to answer are:

1. What are the major effects on wind turbines induced by earthquakes in Iceland?
2. How important is potential seismic exposure when determining design parameters?
3. Do wind turbines behave differently than ordinary building type structures under earthquake excitation?

1.3 Aim and objectives

The aim is to gain insight into the importance of earthquakes on wind power installations. The objective is to give designers recommendations on desirable methodology for assessing the influence of earthquakes on wind turbines.

One of the questions raised is regarding the acceptability of using conventional standard analysis techniques such as those recommended by Eurocode, or are more specific diagnostics methods desired, and under what circumstances should they be used.

The following specific objectives are defined:

1. Building a numerical model of a wind turbine structure
2. Determination of natural frequency and vibration modes
3. Determination of near-field and far-field earthquake response which emphasizes the frequency band that is consistent with the resonant modes of the wind turbine.
4. Discussion on the effect of damping
5. Wind turbine response analysis in parked state.
6. Summary of measurements found in the literature which can be used for calibration and / or test calculation
7. Interpretation of results

1.4 Thesis organization

Chapter 1: The introduction discusses the history of wind turbines and the use of wind energy to generate electricity. The chapter also introduces the seismic risk in Iceland and outlines the aims and objectives of the thesis.

Chapter 2: This chapter gives an overview of existing standards and guidelines used to design wind turbines. The main guidelines reviewed are the RISØ guideline, GL guideline and IEC 61400-1 design requirements. The chapter also gives overview of turbine modelling methods, both simple system models and full system models and existing studies, experimental and numerical of wind turbine response to seismic events.

Chapter 3: The subject of chapter 3 is seismology, explaining the concept of the plate tectonic theory, faults and seismic waves. It also discusses the effects of ground motions both near fault and far fault. Chapter 3.3 gives an overview of earthquakes in Iceland, focusing especially on the South Iceland earthquakes in 2000 and 2008, detailing the strong-motion recordings during the earthquakes in 2000 and 2008.

Chapter 4: This chapter discusses the dynamic analysis and response of Linear Systems, outlining the equation of motion and static condensation as well as soling the equation of motion through undamped free vibration. It also discusses modal analysis and solution methods used to solve the equations, outlining numerical methods and the Newmark Method.

Chapter 5: Chapter 5 gives overview of earthquake response analysis of wind turbine using time series of the recorded ground motion among other information. It gives a description of the wind turbine erected at Búrfell Power station in South Iceland and describes the Matlab modelling workflow used, giving overview of lumped system mass matrix and element stiffness as well as undamped vibration, the selection of seismic data, modal analysis, response history analysis and response spectrum analysis.

Chapter 6: This chapter discusses structural modelling and earthquake analysis, displaying response analysis tables using summary of Seismic response for each earthquake in 2000 and 2008 based on distance to the source of the earthquake. It also discusses the response parameters versus seismic data and the response analysis in SAP, both history analysis and spectrum analysis.

Chapter 7: Concluding remarks include the conclusion of the thesis and discussion on further research needed in the field of the effects of seismic risk to wind turbines.

2 Literature review

2.1 Existing Standards and guidelines

Design requirements and technologies along with components and systems, that have an impact on the function of wind turbines are addressed in wind turbine standards. Three main standards or guidelines provide direct guidance for seismic loading and design of wind turbines:

(1) *Guidelines for Design of Wind Turbines* (Risø, 2001)
(2) *Guideline for the Certification of Wind Turbines* (GL, 2003)
(3) *IEC 61400-1 Ed.3: Wind turbines - Part 1: Design requirements* (IEC, 2005).

GL and Risø standards among other European standards are coordinated with the International Electrotechnical Commission (IEC) standards. The Canadian standards association (CSA) has also adopted the primary IEC standard for wind turbines, IEC 61400-1 (IEC, 2005), while including certain Canadian deviations mostly concerning external conditions (CSA, 2008).

Seismic analysis is only implemented in the design process if the site is in a regions of highly seismic hazard or if it is required by local authorities, since only a few regions throughout the world where seismic loads may be design driving. According to the U.S. Department of Energy 45 GW of wind power capacity was added globally in 2012 with nearly 30 GW added in the United States, India, and China (Wiser & Bolinger, 2013), all countries with large regions of high seismic hazard. A short review will be given in the following chapters on the three guidelines listed above.

2.1.1 Review of RISØ guideline for design of wind turbines

Prior to wind turbine installation various conditions of the site have to be evaluated including environmental aspects like temperature, icing, humidity, solar radiation, corrosion condition and possible earthquake. The guideline for design of wind turbines is a compilation of the knowledge gained over the past years in designing and constructing wind turbines, both researched based projects and practical design experience, but the basis for the guideline is formed from various rules and methods, specifically from the International Electrotechnical Commission (IEC, 2005). The Risø guideline is a collective effort between Det Norske Veritas (DNV) and Risø National Laboratory (Risø) and was founded by the Danish Energy Agency, Det Norske Veritas and Risø National Laboratory.

The Risø guideline provides the most general suggestions with basic instruction associated with seismic loading. A simple SDF model is proposed where the nacelle, rotor, and ¼ of the tower mass are lumped at the top of the tower. The resulting period is then used to select spectral response acceleration from a design response spectrum and therefore determine the seismic loads on the tower.

No recommendation for the appropriate level of damping is provided in Risø guidelines therefore a level of 5% is assumed (ICC, 2006), also no guidance is provided for translating the spectral response acceleration into design load, an appropriate building code procedure will be employed (Risø, 2001).

2.1.2 Review of GL guideline for the Certification of Wind Turbines

The main difference between the GL and the Risø guidelines is that the GL guidelines are prescriptive with detailed guidance on particular aspects of seismic risk. These are consistent with the intent of the publication as a set of requirements for certification.

The guidelines prescribe details of the required seismic analysis.

1. A return period of 475 years is prescribed as the design level earthquake, superimposed with all normal – external loads with a safety factor of 1.0 for the earthquake load.
2. A minimum of 3 modes is required for both time domain and frequency domain analysis, and at least 6 simulations in time domain must be performed per load case.
3. The tower to be considered as elastic, unless characteristics that allow ductile response is present.

No guidance is provided regarding the level of viscous damping, similar to the Risø guidelines (Risø, 2001).

2.1.3 Review of IEC 61400-1 design requirements

The IEC guidelines (IEC, 2005) are similar to the GL guidelines in the way that they focus on prescribing requirements for analysis of seismic loads. As with GL guidelines the design level earthquake is prescribed as a 475 year return event superimposed with the greater of:

- Lifetime averaged operating loads, or
- Emergency shutdown loads.

No earthquake resistance is required for standard class turbines because such events are only design driving in few places in the world, or if a site is already excluded by the local seismic code. For locations where seismic loads can be critical the engineering integrity shall be tested, where evaluation of load shall include combination of seismic loads with a safety factor of 1.0 and other significant, frequently occurring loads. The seismic load is depended on ground acceleration and response spectrum, valuated appropriately. The seismic load evaluation may be carried out through frequency domain methods, in which case, the operational loads are added directly to the seismic load.

2.2 Turbine Modelling Methods

The existing literature on modelling wind turbines for seismic loading can be divided into two types of models. One type is more simplified and focuses on the tower by accounting for the mass of nacelle and rotor as point mass at the top of the tower and thereby removing the complexity of modelling the rotor. The second type of models describes the full turbine, including the nacelle and rotor in details. The first type regards the turbine as a SDOF system and may be unreliable for higher modes than first tower modes.

The second type, full system models, is more flexible but increases the complexity in interpreting the results. These models try to incorporate all possible factors to seismic risk, i.e. aerodynamic loads, rotor dynamics, soil-structure interaction, electrical system dynamics, and other sources. It is also possible to use full system models to predict component loads instead of only tower loads. Designers cannot be certain how a turbine might fail in a seismic event as experience of seismically induced failure in wind turbine has not been systematically documented. The tower and foundation are assumed to by the critical components for seismic loading. This type of numerical model can help evaluate component loads that are not included in a simple tower based model.

Simple system models

As previously discussed, both Risø National Laboratory (Risø, 2001) and the IEC Annex C (IEC, 2005) provide simplified procedures for estimating seismic loading of a wind turbine. Risø guidelines uses simplified model to determine the first tower natural period while IEC assumes the first period based on existing analysis. The first period is then used to retrieve the design response acceleration from the design response spectrum where in Riso the designer selects the appropriate method to translate the design response acceleration into seismic loads, whereas IEC procedure translates the acceleration into a base shear and moment.

Full system models

When the need for further analysis arises such as aerodynamic analysis combined with seismic analysis a full system model is required. Full system models are widely used in the wind energy industry, the two notable modelling tools being GH bladed (Bossanyi, 2003), which is produced by Garrad Hassan (DNV GL) and FAST (Jonkman & Buhl Jr, 2005) which is developed by (NREL). GH and FAST have been validated by Germanischer Lloyd for calculating operational loads associated with typical load cases but other models are also used in the wind industry, such as HAWC2 (Larsen, 2009).

GH bladed uses a limited-degree-of-freedom modal model instead of computationally complex finite model. The major components of the turbine are calculated with modal calculations in the time domain followed by calculation of the resulting nodal forces for each mode. The seismic load can be calculated either by using recorded acceleration time histories or by using synthetic acceleration time history with an elastic response spectrum. The user is able to specify a foundation stiffness to account for soil and foundation influences on the structural response. GH bladed package is able to simulate seismic response with any specified level of damping in combination with other load sources, allowing the designer to explore numerous loading scenarios (Bossanyi, 2003).

FAST uses a combination of modal and multi-body dynamics to simulate the turbine behaviour. The mode shapes are summarized to determine the flexibility of the element in order to calculate the equation of motion using multi-body formulation. FAST does not facilitate seismic loading but allows the user to custom-develop a loading routine at the base of the turbine. However with the appropriate additions to the main software, FAST can provide a full system model for seismic loading (Jonkman & Buhl Jr, 2005).

HAWC2 has been developed since 2003 – 2006 at the aeroelastic design research programme at Risø, National laboratory in Denmark. The structure is calculated using multi-body formulation where the main structure is subdivided into number of Timoshenko beam elements connected with constrains like rigid coupling, a bearing, a prescribed fixed angle etc. The aerodynamics of the model is based on the blade element momentum theory (Larsen, 2009).

2.3 Experimental and numerical studies of wind turbine response

Demand parameters for turbines, such as tower moment demand, are primarily driven by wind excitation and dynamics associated with operation. For that purpose, computational simulation platforms have been developed, such as FAST, maintained by the National Renewable Energy Laboratory (NREL) as described in section 2.2.

Recognizing that wind turbine details are more or less confidential information kept by the manufacturers, National Renewable Energy Laboratory (herein NREL) has developed a numerical 5-MW reference wind turbine as reported in (Jonkman, Butterfield, Musial, & Scott, 2009). This turbine was developed by using any publicly available information on the structural, operational and other aspects of wind turbines that existed at the time. This reference turbine has been used in large number of research studies (Prowell, Elgamal, & Jinchi, 2010), (Prowell, Elgamal, & Jinchi, 2010), among others).

A dynamic field measurement was conducted on a 900 kW turbine installed at Oak Creek Energy Systems (OCES) in the effort of observing the natural frequencies to provide the basis for the development of a model for the FAST code (Prowell et al., 2010).

A 900 kW, 3 bladed upwind turbine with a hub height at 55 meters and a rotor diameter of 53.6 meters has a rotor mass of 16 tons, a nacelle mass of 23 tons and a tower mass of 65 tons making the total mass 104 tons. The turbine foundation is made of hollow cylindrical concrete shell with outer diameter of 3.5 meters and extends 9 meters below the ground surface.

The dynamic response of the turbine was recorded in 15 locations along the height of the tower, 4 on the foundation and 8 locations on the surface of the surrounding soil using a total of 81 channels. Additionally vibration measurements were taken on one of the blades while the rotor rested horizontally on the ground. All of the tower and blade frequencies measured were within the range of interest (0 – 15 Hz) for earthquake loading. The observed first three resonant frequencies for front-aft and side-to-side motion in parked condition are reported in Table 2-1.

Table 2-1. Modelled tower modes for 900kW parked turbine at OakCreek (Prowell et al. 2010)

Mode Type	Orientation	Mean Frequency	Mean Damping
		(Hz)	**(%)**
1st	Side-to-side	0,54	3,4
	Fore-aft	0,56	4,0
2nd	Side-to-side	3,94	1,0
	Fore-aft	4,00	0,9
3rd	Fore-aft	8,86	1,8
	Side-to-side	10,9	0,7

The turbine was simulated using FAST during a parked, operating and emergency shutdown state, with and without the 1940 El Centro earthquake. Many parameters can be evaluated to understand

the response of the turbine to load combinations. Focus on the bending moment demand at the base of the turbine tower. The predominant bending moment was found to be the result of for-aft bending moment due to wind loading. In the earthquake loading simulation two horizontal ground accelerations were utilized, combined using SRSS method.

When independent simulations were combined, a partial safety factor of 1.0 was applied to all the parameters for the earthquake simulation, as mentioned in section 2.1.3. The results show a 12.5 MN-m moment demand for a coupled operating turbine with earthquake as well as parked turbine with earthquake loading only. For the operating case the resulting moment demand increased by 10,1 MN-m to a total of 22,6 MN-m, resulting in a significant difference in demand, which might indicate that the supporting tower might have insufficient capacity based on independent simulations, but be suitable for the coupled simulation. The amplitude of the fore-aft moment demand continued to grow 20 seconds into the earthquake when aerodynamics were not considered but stopped growing 10 seconds after the onset of shaking otherwise. This combined demand suggests that the increase in damping due to aerodynamic loads results in a lower overall demand. Such implications could clearly affect the economic viability of wind energy in regions with a high seismic hazard (Prowell I. , Elgamal, Romanowitz, Duggan, & Jonkman, 2010).

A full-scale test was planned and conducted at the University of California, San Diego (UCSD) by A. Elgamal, J. Restrepo, and M. Veletzos (Prowell et al., 2010) where an actual 65-kW wind turbine was subjected to base excitation using the Network for Earthquake Engineering Simulation (NEES) Large High Performance Outdoor Shake Table (LHPOST). This experiment provided a baseline for seismic behaviour of a parked turbine in low winds, recognizing that experimental validation is currently scarce.

3 Earthquakes

3.1 Seismology

3.1.1 Plate tectonic theory

A large – scale tectonic processes, referred to as 'plate tectonics' are what causes earthquake occurrences. The theory derives from the theory of continental drift and sea – floor spreading. By observation, seismic activity occurs predominantly on known plate boundaries as shown in Figure 3-1, promotes that earthquakes are now acknowledged to be symptoms of active tectonic movements (Scholz, 1990).

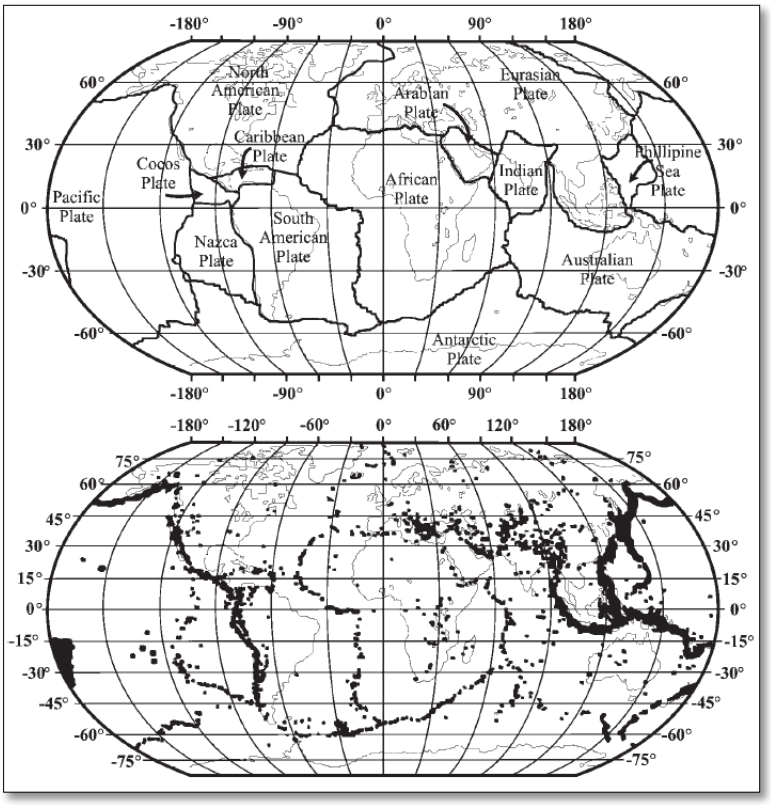

Figure 3-1. Tectonic plates (left) and worldwide earthquake distribution (right) (Elnashai & Sarno, 2008).

Plates forming the crust or lithosphere among part of the mantle of the earth is a stable rigid rock slabs with thickness of about 100 km. The crust has a complex geological structure and a non-uniform thickness of 25 – 60 km under continents and 4 – 6 km under ocean. At a depth of 50 km in the upper mantle a 400 km thick layer of lithosphere moves horizontally. This movement is caused by convection currents in the mantle with a velocity at about 1 – 10 cm/year. The lithosphere is divided into 15 rigid plates according to the theory of continental drift. Large tectonic forces take place at the edges, known as plate boundaries, due to the relative movement of the lithosphere – asthenosphere complex.

The principal types of plate boundaries can be grouped as follows:

- **Divergent or rift zones:**
  Plates separate themselves from one another leading to effusion of magma or the lithosphere diverges from the interior of the Earth.
- **Convergent or subduction zones**
  Adjacent plates converge and collide. A subduction process carries the slab-like plate, known as the 'under-thrusting plate' into a dipping zone.
- **Transform zones or trans current horizontal slip**
  Two plates glide past one another but without creating new lithosphere or subducting old lithosphere.

Continental drift is the movement of continents over the Earth's surface as well as their change in position relative to each other. Shallow and intermediate earthquakes occur at convergent zones in bands of hundreds of kilometres wide and can be very large, for example the 1897 Assam (India) (Richter, 1958). The creation of new oceanic crust at mid-ocean ridges is called sea-floor spreading where the crust moves away from the ridges and divergent plate boundaries form narrow bands of moderate shallow earthquakes (Elnashai & Sarno, 2008).

Contributing 95% of worldwide seismic energy release, plate boundary, also known as inter – plate earthquake, is provided geological explanation through plate tectonic theory. However earthquakes are not confined to plate boundaries. Intra – plate, a local small magnitude earthquake can cause considerable damage. Examples of such devastating events are well documented (Scholz, 1990) (Bolt, 1999), among others.

The origin of the rupture is represented by a point called focus or hypocentre. The projection of the focus on the surface is called epicentre and they are located by geographical coordinates. Descriptions of the source parameters can be seen in Figure 3-2, namely epicentral distance, hypocentral or focal distance, and focal depth. When earthquake is generated by sudden fault slip seismic waves travel from the focal point and is observed at a site located at the epicentral distance.

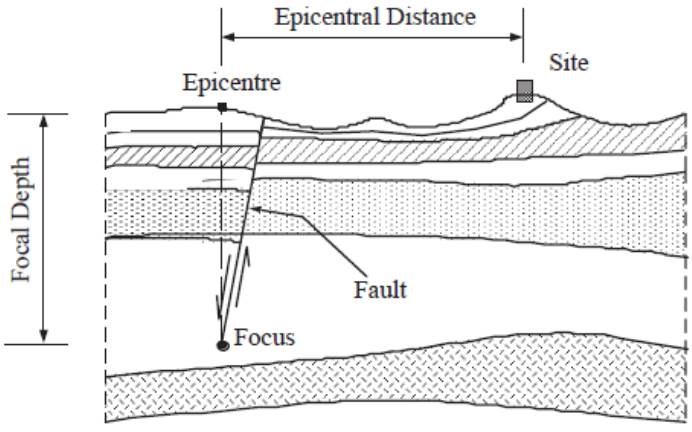

Figure 3-2. Definition of source parameters (Elnashai & Sarno, 2008).

Three types of earthquakes are referred to as shallow, intermediate and deep focus. Earthquakes occurring at a depth of 5 – 15 km are called shallow while intermediate earthquakes are at a depth of 20 – 50 km, thirdly deep earthquakes occur at a depth of 300 – 700 km underground. Earthquakes occur normally at a depth of 5 – 15 km, intermediate earthquakes have foci at about 20 – 50 km and deep earthquakes occasionally at a depth of several hundred kilometres. Crustal earthquakes normally have depths of about 30 km or less. For example, in Iceland the majority of earthquakes have focal depths in the upper 5 – 10 km (Elnashai & Sarno, 2008).

3.1.2 Faults

Elastic strain energy builds up and suddenly releases through the rupture of the interface zone as the groundmasses move with respect to one another. As the distorted plates snap back towards equilibrium an earthquake ground motion is produced. This process is referred to as elastic rebound and the resulting fracture in the Earth's crust is known as the fault. During the sudden rupture, seismic waves are generated and travel away from the source along the Earth's outer layer with varying velocity depending on the characteristics of the material trough which they travel.

Most earthquakes occur at tectonic plate boundaries but many faults occur far from them, and in fact faults usually do not consist of a single clean fracture rather a zone of complex deformation associated with the fault plane. The two sides of a fault are called the hanging wall and footwall. By definition, the hanging wall occurs above the fault and the footwall occurs below the fault.

Slip mechanism of active faults affects the characteristics of the earthquake ground motions therefore active faults may be classified on the basis of their geometry and the direction of relative slip. Three angles define the orientation of the fault, Azimuth, Dip and Slip (or Rake). As displayed in Figure 3-3 the dimension of these angles are given by its area S and the fault slip is measured by the relative displacement Δu (Elnashai & Sarno, 2008).

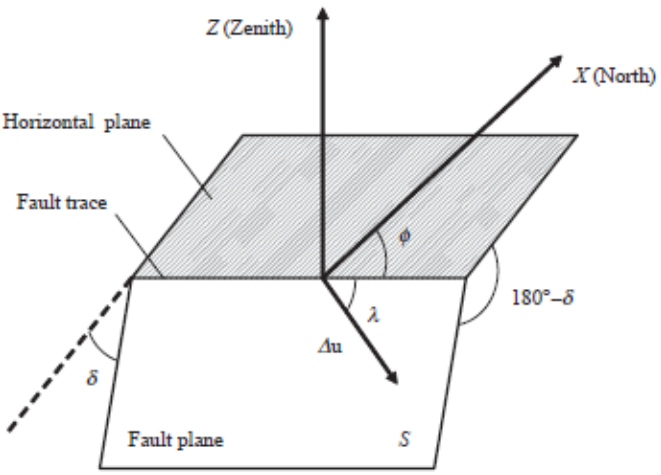

Figure 3-3. Parameters used to describe fault motion (Elnashai & Sarno, 2008).

The parameters used to describe fault motion and its dimensions are as follows:

Azimuth($\boldsymbol{\phi}$):

The angle between the trace of the fault, i.e. the intersection of the fault plane with the horizontal, and the northerly direction ($0\,^\circ \leq \varphi \leq 360\,^\circ$). The angle is measured so that the fault plane dips to the right - hand side.

Dip($\boldsymbol{\delta}$):

The angle between the fault and the horizontal plane ($0° \leq \delta \leq 90°$).

Slip or rake($\boldsymbol{\lambda}$):

The angle between the direction of relative displacement and the horizontal direction ($-180\,^\circ \leq \lambda \leq 180°$). It is measured on the fault plane.

Relative displacement($\boldsymbol{\Delta u}$):

The distance travelled by a point on either side of the fault plane. If Δu varies along the fault plane, its mean value is generally used

Area($\boldsymbol{S}$):

Surface area of the highly stressed region within the fault plane.

Faults can be categorized into three groups based on the sense of slip. Main movement on the fault plane is vertical is known as Dip-slip fault but when the movement is in the horizontal direction the fault is known as a transform-slip or strike-slip. In some cases significant components of both strike and dip slip occur together known as Oblique-slip (Bommer J. J., 2001). Different types of faults produce different types of ground motion and many studies show difference in strong ground motion due to the focal mechanism of the earthquake, for example reverse faulting is believed to produce larger amplitude ground motion than those from strike-slip earthquakes e.g. (Bommer, Douglas, & Strasser, 2003)

Dip-slip

When blocks move vertically with respect to one another a dip-slip effect occurs, Figure 3-4. If the footwall i.e. the block underlying the fault plane moves up the dip and away from the hanging wall, normal faults are obtained causing shearing failure due to tensile forces. In turn when the hanging wall moves upward in relation to the footwall, the faults are reversed leading to compressive forces (Elnashai & Sarno, 2008).

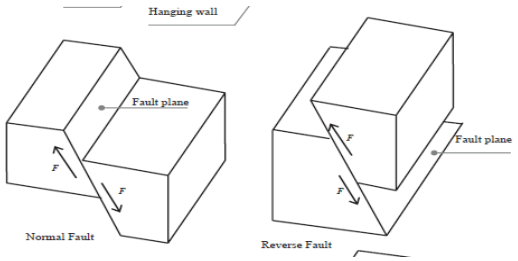

Figure 3-4. Normal Dip slip fault (left) and reverse (right)
(Elnashai & Sarno, 2008).

Strike-slip

A strike slip effect occurs when blocks move horizontally past one another Figure 3-5. The movement can be right – lateral or left – lateral, depending on the sense of the lateral motion of the blocks for an observer located on one side of the fault line. The slip can be caused by either compression or tension stresses along as essentially vertical fault plane (Elnashai & Sarno, 2008).

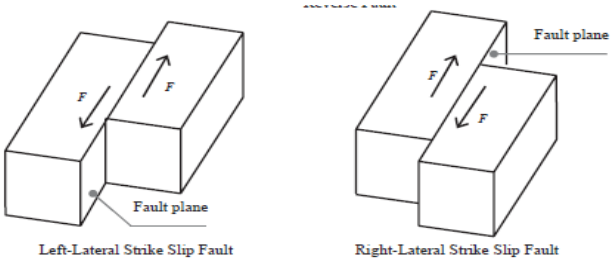

Figure 3-5. Fundamental fault mechanisms
(Elnashai & Sarno, 2008).

Oblique-slip faults

A combination of strike-slip and dip-slip movements are called oblique slip Figure 3-6. They can be either normal or reverse and right- or left-lateral. Nearly all faults have some components of strike- and dip-slip, so defining a fault as oblique requires both components to be measurable and significant (Bommer J. J., 2001).

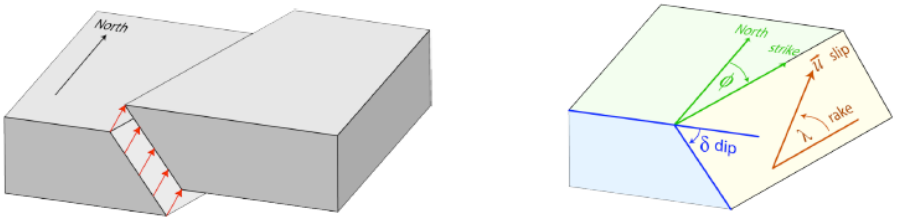

Figure 3-6. Oblique slip fault, (Bommer J. J., 2001).

3.1.3 Seismic waves

Earthquake shaking, as fault ruptures are caused by brittle fractures of the crust, are generated by two types of elastic seismic waves known as body and surface waves. The shaking felt is generally a combination of these waves, especially at small distances from the source or "near - field".

Body waves are longitudinal waves or P – waves that cause alternate push (compression) and pull (tension) in the surface and have relatively little damage potential, and transverse waves or S – waves that causes vertical and horizontal side – to – side motion, see Figure 3-7. S – waves are also known as "shear waves" since they contribute to the shear stresses in the rock along their paths and can be split into horizontal (SH) and vertical (SV) components, both of which can cause significant damage (Elnashai & Sarno, 2008).

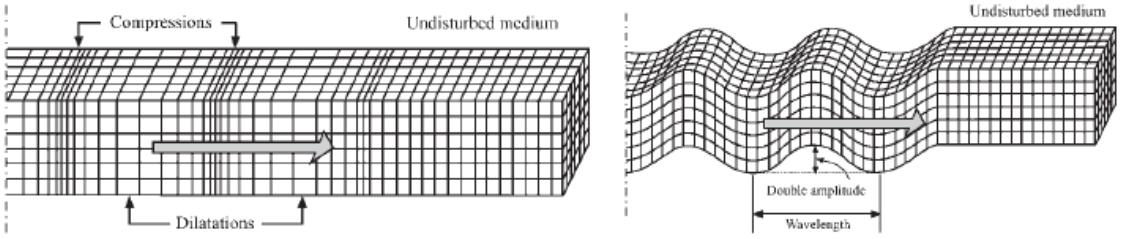

Figure 3-7. Travel path mechanisms of body waves:
Primary waves (left) and secondary waves (right) (Elnashai & Sarno, 2008).

The actual speed of body waves depends upon the density and elastic properties of the rock and soil through which they pass. P – waves travel at speeds between 1.5 and 8 kilometres per second while S – waves are analogous to electromagnetic waves, show large amplitudes and long periods and cannot propagate in fluids. As described by Navier's equation e.g. (Udias, 1999), the propagation velocities of P - and S – waves within an isotropic elastic medium with density ρ , denoted as v_p and v_s respectively, are as follows:

$$v_p = \sqrt{\frac{E(1-\upsilon)}{\rho(1+\upsilon)(1-2\upsilon)}} \tag{3-1}$$

$$v_s = \sqrt{\frac{E}{2\rho(1+\upsilon)}} \tag{3-2}$$

in which υ is Poisson's ratio and E is Young's modulus of the elastic medium.

At the earth's surface body waves are polarized and become surface waves. Surface waves include Love waves indicated as "L" and Rayleigh waves indicated as "R" (Elnashai & Sarno, 2008). Rayleigh wave is a vertical wave that moves similar to ripples in water, as seen in Figure 3-8, while Love waves cause lateral movements of the earth in a motion like a moving snake (Srbulov, 2010).

Love and Rayleigh waves are more distinct at distances further away from the earthquake source, unlike body waves that are equally well represented in earthquakes at all depths, surface waves are most prominent in shallow earthquakes. (Elnashai & Sarno, 2008). Due to the different characteristics and different combination of wave motion depending on distance to source, it is now common practice, on major engineering projects, to investigate several different sets of ground motions to consider both near fault and far fault events.

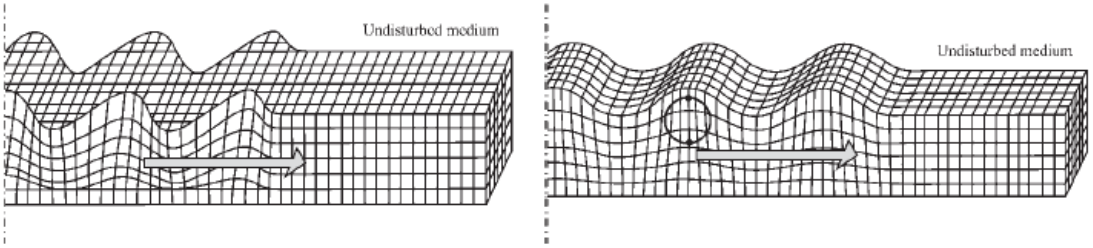

Figure 3-8. Travel path mechanisms of surface waves:
Love waves (left) and Rayleigh waves (right) (Elnashai & Sarno, 2008).

3.2 Earthquakes in Iceland

Earthquakes occurring in Iceland can be dated since the settlement and are mainly located at the southern lowlands and at the continental shelf in North Iceland. Earthquake descriptions before 1896 can only be found in historical literature, for instance by Jónas Hallgrímsson, poet and naturalist and Þorvaldur Thoroddsen geographer but they based their work on Icelandic logs and medieval literature. After the year 1896, all the major seismic activities were recorded as has been documented by (Ambraseys & Sigbjörnsson, 2000). As we progress to the 20th century, instruments producing seismic records increase steadily (Sólnes, Sigmundsson, & Bessason, 2013).

Iceland is located in the North Atlantic Ocean at the junction of Mid-Atlantic Ridge and the Greenland–Iceland–Faeroe Ridge (Guðmundsson, 2000). The seismic activity in Iceland is primarily related to the Mid-Atlantic Ridge where it crosses the island shifting it eastward trough two major fracture zones, the South Iceland Seismic zone in the south, and Tjornes Fracture Zone in the north. Within these two zones all major damaging earthquakes have originated however outside their area, significant seismic activity occurs but is primarily related to volcanoes.

3.2.1 South Iceland Earthquake 2000

On June 17th 2000 a damaging earthquake, with a moment magnitude of 6.5 (Global CMT Catalog, 2007), began in South Iceland and an epicentre just north of the rural village of Hella Figure 3-9. Major Seismic activity followed throughout the South Iceland seismic zone including the area northwest part of Hveragerði named Hengill and at the Reykjanes Peninsula.

The second earthquake in the sequence occurred on June 21st, with a moment magnitude of 6.4, placed approximately 17 km west of the epicentre of the former event (Global CMT Catalog, 2007). In Figure 3-9, an overview of the epicentre location along with approximate surface traces of the causative fault and location of strong-motion stations in the near-fault area can be seen (Sigbjörnsson & Ólafsson, 2004).

The damage of the earthquakes in June 2000 was widespread but major damage was mostly confined to the epicentral region of the two large earthquakes on 17 June and 21 June. The damage area of the first earthquake was estimated to spread over 440 km2, affecting mostly individuals and entities in the rural village of Hella. Hella is situated no more than 5 km from the south end of the fault. The damage area of the second earthquake in June 2000 was about 360 km^2, damaging mostly buildings, individual farms, groups of summer cottages and infrastructure, in the epicentral area (Sigbjörnsson, Ólafsson, & Snæbjörnsson, 2007).

3.2.2 South Iceland Earthquake 2008

Thursday 29 May 2008 at 15:45 an earthquake shook South Iceland, the epicentre was in the Ölfus District, between Selfoss and Hveragerði. The moment magnitude of the earthquake was 6.3 according to the Global Centroid Moment Tensor (CMT) database1 and the Instituto Nazionale di Geofisica e Vulcanologia (INGV). The event had similar characteristics to the earthquakes in June 2000, a shallow crustal earthquake on a north-south trending right-lateral strike slip fault. (Ambraseys, et al., 2004); (Sigbjörnsson & Ólafsson, On the South Iceland earthquake in June 2000, 2004); (Sigbjörnsson, Ólafsson, & Snæbjörnsson, Macroseismic effects related to strong ground motion: a study of the South Iceland earthquakes in June 2000, 2007); (Halldórsson, Ólafsson, & Sigbjörnsson, 2007). The damage of the event was widespread and significant, recorded acceleration in the epicentral area even have exceeded the codified design loading. Majority of the buildings, however, withstood the high accelerations without visible damage but damage to household articles and build contents was extensive in the near fault region. The earthquake affected geothermal areas, forming new hot springs. During the earthquake no interruption of electricity supple occurred. Seismic activity in the wake of the earthquake had impact and produced numerous events that may have augmented the structural damage in the area (Ákason, Ólafsson, & Sigbjörnsson, 2006a); (Ákason, Ólafsson, & Sigbjörnsson, 2006b).

3.2.3 Strong-motion recordings

The earthquake analysis in this study are based of recordings from June 2000 and 2008 earthquakes in South Iceland that are accessible within the framework of the ISESD project (Internet-Site for European Strong-Motion Data), supported by the European Commission, Research-Directorate General, Environment and Climate Programme (Ambraseys et al. 2004). Both uncorrected and corrected three component strong-motion acceleration records can be accessed at the website as well as corresponding (linear elastic) response spectra and information on seismological, instrumental and site-specific parameters.

The University of Iceland-Earthquake Engineering Research Centre (UI-EERC) operates the Icelandic Strong-Motion Network, under agreements with the National Power Company and the municipalities in South and North Iceland. The network relies on 36 free field ground response stations in addition to arrays in buildings and structures, see Figure 3-9.

In June 2000 and the following months the network recorded a total of 83 events, the biggest ones on 17 and 21 June - which were recorded at every operational station within a radius of 150 km. The highest recorded PGAs were 0,64g and 0,84g, showing that the acceleration in the near source area was substantial and even greater that would have been expected from earthquakes of this magnitude (Sigbjörnsson, Ólafsson, & Snæbjörnsson, 2007).

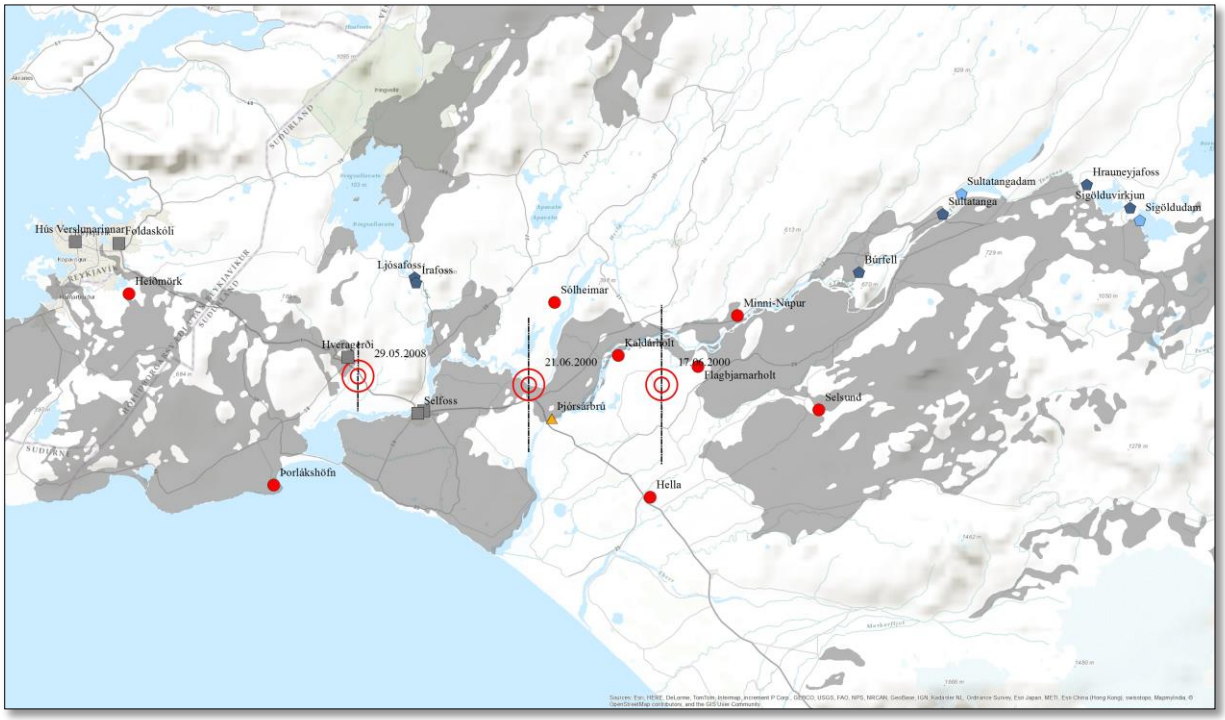

Figure 3-9. Epicentral location of the South Iceland earthquakes in June 2000 and May 2008, and overview of strong-motion stations in the near-fault area. Epicentres are indicated by stars and approximate surface traces of the causative faults by dashed lines. The following notation is used for the strong-motion stations: red circle = ground response station; yellow triangle = bridge; blue triangle = hydropower station; cyan triangle = dam; grey square = building.

The earthquake in South Iceland May 2008 was also recorded by the Icelandic Strong-motion Network as well as the newly installed ICEARRAY network (Halldórsson et al. 2008), which is a small-aperture array located in the epicentral area. Near the epicentre the PGA recorded was high, with indication that the vertical acceleration even exceeding 1g. In the Selfoss, towards southeast of the epicentre, horizontal acceleration reached 0,5g. Northwest of the epicentre, in Hveragerði, horizontal and the corresponding vertical acceleration reached 0,85g at some locations. More than 40 km from the epicentre, in Reykjavík, the PGA was less than 0,4g.

Figure 3-9 shows geographical overview of the location of the strong-motion stations and epicentres of the event in May 2008 and the two events in June 2000. No clear indications of a single causative fault can be found on the surface. That fact can partly be explained by thick sediments overlying the bedrock. The records also show that the recorded earthquake waves were generated by two parallel faults, the initial rupture being north-south trending fault and the second one, 1 second later, on another north-south trending fault approximately 3.5 km west of the first one. The aftershocks records also indicate north-south trending faults (Sigbjörnsson, Snæbjörnsson, Higgins, Halldórsson, & Ólafsson, 2009). The ISESD database contains 24 stations that recorded the ground motion on June 17th and 21st 2000, and 8 stations that recorded on May 29th 2008.

4 Dynamic analysis and response of Linear Systems

4.1 Equation of motion

A system consists of a mass m concentrated at element joint, a frame that provides stiffness to the system and a viscous damper that dissipates vibrational energy of the system. Each structural member contributes to the inertia (mass), elasticity (stiffness of flexibility), and energy dissipation (damping) properties. These properties can be considered as separate components (Chopra, 2007):

- Mass component
- Stiffness component
- Damping component

Forces $p_j(t)$ acting on each point mass m_j has a resisting force f_S, and the damping force f_D acting against them. Newton's second law of motion gives for each mass:

$$p_j - f_{Sj} - f_{Dj} = m_j \ddot{u}_j \quad \text{or} \quad m_j \ddot{u}_j + f_{Dj} + f_{Sj} = p_j(t) \tag{4-1}$$

Given that Equation (4-1) contains two equations for $j = 1$ and 2, it can be rewritten as:

$$\begin{bmatrix} m_1 & 0 \\ 0 & m_2 \end{bmatrix} \begin{Bmatrix} \ddot{u}_1 \\ \ddot{u}_2 \end{Bmatrix} + \begin{Bmatrix} f_{D1} \\ f_{D2} \end{Bmatrix} + \begin{Bmatrix} f_{S1} \\ f_{S1} \end{Bmatrix} = \begin{Bmatrix} p_1(t) \\ p_2(t) \end{Bmatrix} \tag{4-2}$$

Or written compactly as:

$$\boldsymbol{m\ddot{u}} + \boldsymbol{f}_D + \boldsymbol{f}_S = \boldsymbol{p}(t) \tag{4-3}$$

Where $\boldsymbol{m\ddot{u}}$ is the inertia force and the damping force $\boldsymbol{f_D}$ is related to the velocity $\dot{u}$ across the linear viscous damper by

$$\begin{Bmatrix} f_{D1} \\ f_{D2} \end{Bmatrix} = \begin{bmatrix} c_1 + c_2 & -c_2 \\ -c_2 & c_2 \end{bmatrix} \begin{Bmatrix} \dot{u}_1 \\ \dot{u}_2 \end{Bmatrix} \quad \text{or} \quad f_D = c\dot{u} \tag{4-4}$$

The relationship between the lateral force f_s and resulting deformation u in linear system can be described as

$$\begin{Bmatrix} f_{S1} \\ f_{S2} \end{Bmatrix} = \begin{bmatrix} k_1 + k_2 & -k_2 \\ -k_2 & k_2 \end{bmatrix} \begin{Bmatrix} u_1 \\ u_2 \end{Bmatrix} \quad \text{or} \quad f_s = ku \tag{4-5}$$

where k is the lateral stiffness of the system.

Substituting Eg. (4-4) and (4-5) into Eq. (4-3) gives.

$$\boldsymbol{m\ddot{u}} + \boldsymbol{c\dot{u}} + \boldsymbol{ku} = \boldsymbol{p}(t) \tag{4-6}$$

4.1.1 Static condensation

The static condensation method is used to eliminate from dynamic analysis those DOFs of a structure to which zero mass is assigned; however, all the DOFs are included in the static analysis.

Typically the mass of the structure is idealized as concentrated in point lumps at the nodes, and the mass matrix contains zero diagonal elements in the rotational DOFs. These are the DOFs that can be eliminated from the dynamic analysis of the structure provided that the dynamic excitation does not include any external forces in the rotational DOFs, as in the case of earthquake excitation.

Even if included in formulating the stiffness matrix. the vertical DOFs of the building can also be eliminated from dynamic analysis-because the inertial effects associated with the vertical DOFs of building frames are usually small-provided that the dynamic excitation does not include vertical forces at the nodes, as in the case of horizontal ground motion. The equations of motion for a system excluding damping are written in partitioned form (Chopra, 2007):

$$m_{tt}u_t + k_{tt}u_t + k_{t0}u_0 = p_t(t) \quad k_{0t}u_t + k_{00}u_0 = 0 \tag{4-7}$$

Because no inertia terms or external forces are associated with u_0, A static relationship between u_0 and u_t $is\ permited$:

$$u_0 = -k_{00}^{-1}k_{0t}u_t \tag{4-8}$$

Therefore

$$m_{tt}u_t + \hat{k}_{tt}u_t = p_t(t) \tag{4-9}$$

Where $\hat{k}_{tt}$ is the condensed stiffness matrix given by:

$$\hat{k}_{tt} = k_{tt} - k_{0t}^{T}k_{00}^{-1}k_{0t} \tag{4-10}$$

4.2 Solving the equation of motion

4.2.1 Free vibration

Undamped free vibration

When a structure is allowed to vibrate without any external dynamic excitation it is said to undergo *free vibration*. Studying free vibration leads to the notation of natural vibration frequency and damping ratio for an SDF system and how the damping ratio controls the rate at which the motion decays. Free vibration is initiated by disturbing the system from its static equilibrium position by imparting the mass some displacement $u(0)$ and velocity $\dot{u}(0)$ at time zero. Subject to these inital conditions, the solution to the homogeneous differential equation is known as the simple harmonic motion.

$$u(t) = u(0)\cos\omega_n t + \frac{\dot{u}(0)}{\omega_n}\sin\omega_n t \tag{4-11}$$

Where

$$\omega_n = \sqrt{\frac{k}{m}}\ (rad/sec) \tag{4-12}$$

One cycle of free vibration is the natural period of vibration T_n, in units of seconds and is related to the natural circular frequency of vibration, ω_n, in units of radians per second.

$$T_n = \frac{2\pi}{\omega_n}\ (sec) \tag{4-13}$$

The natural cyclic frequency of vibration executes $1/T_n$ cycles in 1 second, in units of Hertz (Hz).

$$f_n = \frac{1}{T_n}\ (Hz) \tag{4-14}$$

The natural vibration properties ω_n, T_n and f_n depend only on the mass and stiffness of the structure. Of two SDF system having the same mass but different stiffness will have the higher natural frequency and the shorter natural period. Similarly the heavier of two structures having the same stiffness will have the lower natural frequency and the longer natural period. Because the system is linear, these vibration properties are independent of the initial displacement and velocity (Chopra, 2007).

4.2.2 Modal analysis

In classical modal analysis procedure, the equations of motion are transformed to modal coordinates. Each uncoupled modal equation is solved to determine the modal contributions to the response. Finally the modal responses are summarized to obtain the total response.

Each mode has its own particular pattern of deformation based on a specific natural mode of vibration ϕ_n, a natural frequency of vibration ω_n, and the modal damping ratio ζ_n.

The method of modal combination is however only valid for earthquake analysis of structures responding within their linear elastic range, as non-linear behaviour results in changes in the stiffness and damping parameters (Chopra, 2007).

When the displacement vector u of an MDF system is expanded in terms of modal contributions the dynamic response can be expressed as

$$\boldsymbol{u}(t) = \sum_{r=1}^{N} \phi_r q_r(t) = \boldsymbol{\Phi q}(t) \tag{4-15}$$

Transforming the equation of motion to uncoupled equations with coordinates $q_n(t)$ as the unknowns and premultiplying each term by ϕ_n gives

$$\sum_{r=1}^{N} \phi_n^T \boldsymbol{m} \phi_r q_r(t) + \sum_{r=1}^{N} \phi_n^T \boldsymbol{k} q_r(t) = \phi_n^T \boldsymbol{p}(\boldsymbol{t}) \tag{4-16}$$

Due to orthogonality all the terms in each of the summations vanish, except when $r = n$, therfore reducing the equation to

$$M_n \ddot{q}_n(t) + K_n q_n(t) = P_n(t) \tag{4-17}$$

where

$$M_n = \phi_n^T \cdot \boldsymbol{m} \cdot \phi_n \qquad K_n = \phi_n^T \cdot \boldsymbol{k} \cdot \phi_n \qquad P_n(t) = \phi_n^T \cdot \boldsymbol{p}(t) \tag{4-18}$$

The effective earthquake forces $p_{eff}(t)$ can be expressed as a spatial distribution defined by $s = m\iota$. This spatial distribution can be expanded as a summation of modal inertia force distribution s_n.

$$\boldsymbol{m}\iota = \sum_{\mathrm{n}=1}^{\mathrm{N}} s_n = \sum_{\mathrm{n}=1}^{\mathrm{N}} \Gamma_n \boldsymbol{m} \phi_n \tag{4-19}$$

where

$$\Gamma_n = \frac{L_n}{M_n} \qquad L_n = \phi_n^T \boldsymbol{m}\iota \qquad M_n = \phi_n^T \boldsymbol{m} \phi_n \tag{4-20}$$

4.2.3 Modal response

The response of the MDF system to $p_{eff}(t)$ is defined within a single mode where the mass or floor displacements are:

$$u_{jn}(t) = \Gamma_n \phi_{jn} D_n(t) \tag{4-21}$$

The difference in displacement between adjacent mass-points or ajacent floor levels is defined as the drift, i.e.:

$$\Delta_{jn}(t) = u_{jn}(t) - u_{j-1,n}(t) = \Gamma_n \left(\phi_{jn} - \phi_{j-1,n}\right) D_n(t) \tag{4-22}$$

The equivalent static forces $f_n(t)$ for the n^{th} mode are

$$f_n(t) = s_n A_n(t) \quad f_{jn}(t) = s_{jn} A_n(t) \tag{4-23}$$

The response quantity $r(t)$, which can represent the internal element forces can be expressed as

$$r_n(t) = r_n^{st} A_n(t) \tag{4-24}$$

Where r_n^{st} denotes the modal static response and $A_n(t)$ is the pseudo-acceleration response of the n^{th} mode.

$$A_n(t) = \omega_n^2 D_n(t) \tag{4-25}$$

4.2.4 Global response

Response History Approach

The total (global) earthquake response time-history for the system is a combination of modal responses (Chopra, 2007). The following two equations provide relations to evaluate the nodal displacements and the response quantity *r*(*t*), which can represent the internal element forces.

$$u(t) = \sum_{n=1}^{N} u_n(t) = \sum_{n=1}^{N} \Gamma_n \Phi_{jn} D_n(t) \tag{4-26}$$

$$r(t) = \sum_{n=1}^{N} r_n(t) = \sum_{n=1}^{N} r_n^{st} A_n(t) \tag{4-27}$$

Response Spectrum Approach

The maximum earthquake response for the system can be evaluated through a combination modal responses based on a response spectrum providing the maximum modal response $\langle A_n(t)\rangle_{max}$, for each mode. The simplest representation is a direct summation as shown in Eq.(4-28), but a more common and realistic approach is to use the Square Root of Sum of Squares (SRSS) combination approach or the Complete Quadratic Combination (CQC) approach, see Chopra (2007).

$$\langle D(t)\rangle_{max} = \sum_{n=1}^{N} \langle D_n(t)\rangle_{max} = \sum_{n=1}^{N} \Gamma_n \Phi_{jn} \langle D_n(t)\rangle_{max} \tag{4-28}$$

4.2.5 Solution methods

Of all the methods used to solve differential equations, numerical integration methods are generally the most appropriate option when it comes to seismic analysis. Other methods like the Duhamel's Integral or the Frequency – Domain Method are widely used in solving the differential equation, but they are only valid for linear response analysis. The only practical approach for systems affected by inelastic behaviour during intense earthquakes involves numerical time – stepping methods.

Numerical Methods

Numerical time-stepping methods are used for integration of differential equation. These methods arise have a broad application in applied mechanics. Herein, the basic methods used in dynamic response analysis, are briefly introduced.

For an inelastic system the equation of motion to be solved numerically is

$$m\ddot{u} + c\dot{u} + fs(u,\dot{u}) = p(t) \quad or \quad -m\ddot{u}_g(t) \tag{4-29}$$

Subject to the initial conditions

$$u_0 = u(0) \qquad \dot{u}_0 = \dot{u}(0) \tag{4-30}$$

A linear viscous damping is normally assumed but due to lack of information on damping, especially at large amplitudes of motions it is rarely considered. The applied force $p(t)$ is given by a set of discrete values, $p_i = p(t_i), \quad i = 0\ to\ N$.

$$\Delta t_i = t_i + 1 - t_i \tag{4-31}$$

The response is determined at discrete instant t_i, denoted as time i. The displacement, velocity, and acceleration of the sDF system are u_i, $\dot{u}_i$, and $\ddot{u}_i$, respectively. These values, assumed to be known satisfy Eq. (4-29) at time i:

$$m\ddot{u}_i + c\dot{u}_i + (fs)_i = p_i \tag{4-32}$$

Where $(fs)_i$ is the resisting force at time i; $(fs)_i = ku_i$ for a linearly elastic system (Chopra, 2007).

With numerical procedures, response quantities u_{i+1}, $\dot{u}_{i+1}$, and $\ddot{u}_{i+1}$, at the time $i+1$ can be determined that satisfy Eq. (4-29) at time i.

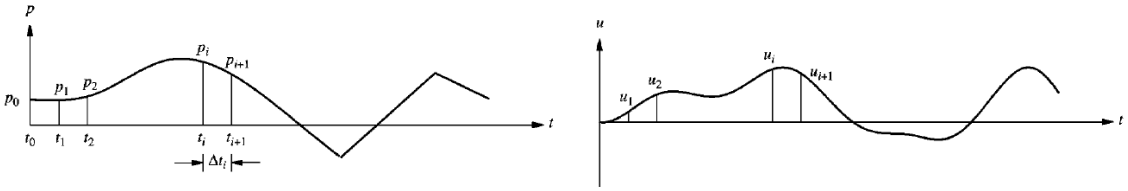

Figure 4-1. Notation for time-stepping method.

The time – stepping procedure gives the desired response at instant of time $i = 1,2,3,\ldots$, when applied successively with $i = 0,1,2,3,...$, provided that the initial conditions are known. The stepping interval from time i to i+1 does not have to be constant and many approximate procedures are can be implemented numerically.

$$m\ddot{u}_{i+1} + c\dot{u}_{i+1} + (fs)_{i+1} = p_{i+1} \tag{4-33}$$

There are three important requirements for a numerical procedure:

1. **Convergence**
   As the time step decreases, the numerical solution should approach the exact solution.
2. **Stability**
   The numerical solution should be stable in the presence of numerical round-off errors.
3. **Accuracy**
   The numerical procedure should provide results that are close enough to the exact solution.

Among the time-stepping procedures, are methods based on interpolation of the excitation function, methods based on finite difference expressions of velocity and acceleration, and methods based on assumed variation of acceleration, which is well suited to evaluate seismic response.

The Newmark Method

The year 1959, N. M. Newmark developed a family of time-stepping methods presented by the following equations:

$$\dot{u}_{i+1} = \dot{u}_i + [(1-\gamma)\Delta t]\ddot{u}_i + (\gamma\Delta t)\ddot{u}_{i+1} \tag{4-34}$$

$$u_{i+1} = u_i + (\Delta t)\dot{u}_i + [(0.5-\beta)(\Delta t)^2]\ddot{u}_i + [\beta(\Delta t)^2]\ddot{u}_{i+1} \tag{4-35}$$

The parameters β and γ define the variation of acceleration over each time step and determine the stability and accuracy characteristics of the method chosen (Chopra, 2007).

4.3 Earthquake Response of linear systems

4.3.1 Formulation of the equation of motion

Because most structures are designed with the expectation that they will deform beyond the linearly elastic limit during major, infrequent earthquakes see chapter 7.

The principal problem of structural dynamics in earthquake-prone regions is the behaviour of structures subjected to earthquake-induced motion of the base of the structure. The ground displacement denoted by u_g and the relative displacement u between the mass and the ground are related at each instant of time by:

$$u^t(t) = u(t) + u_g(t) \tag{4-36}$$

Both displacements refer to the same inertial frame of reference and their positive direction coincides. Using the concept of dynamic equilibrium including the inertia force f_I the equation of dynamic equilibrium is

$$f_I + f_D + f_S = 0 \tag{4-37}$$

The relative motion u due to structural deforamtion produces elastic and damping forces. Thus for a linear system Newtowns second law of motion is still valid. The inertia force f_I is related to the acceleration $\ddot{u}^t$ of the mass and the ground motion can be replaced by the effective earthquake force.

$$p_{eff}(t)) = -m\ddot{u}_g(t) \tag{4-38}$$

The equation of motion governing the relative displacement of deformation $u(t)$ of the linear structure subjected to ground acceleration $\ddot{u}_g(t)$ is

$$m\ddot{u} + c\dot{u} + ku = -m\ddot{u}_g(t) \tag{4-39}$$

Looking at the equation of motion that governs the response of an MDF system to earthquake induced ground motion, the resultant force $\boldsymbol{p}_{eff}(t)$ can be described as,

$$\boldsymbol{p_{eff}}(t) = -\boldsymbol{m\iota}\ddot{u}_g(t) \tag{4-40}$$

where $\boldsymbol{m}$ is the mass matrix and $\boldsymbol{\iota}$ is the influence vector.

The quasi-static displacment can be expressed as $u^s(t) = \boldsymbol{\iota} u_g(t)$, where the influence vector $\boldsymbol{\iota}$ represents the displacements of the masses resulting from static application of a unit ground displacement; thus

$$\boldsymbol{u}^t(t) = \boldsymbol{\iota} u_g(t) + \boldsymbol{u}(t) \tag{4-41}$$

Procedures for earthquake analysis are developed in two different ways. The response history analysis (RHA) is used to calculate structural response as a function of time when the system is subjected to a given ground acceleration $\ddot{u}_g(t)$. This can be achieved using numerical integration schemes as presented in section 4.2.5. On the other hand the response spectrum analysis (RSA)

computes the peak response of a structure during an earthquake directly from the earthquake response spectrum, not needing the response history. The latter process does not predict exact peak response, however it provides an estimate of the peak response that is sufficiently accurate for structural design application. The Response spectrum a approach is outlined in the following section.

4.3.2 Response Spectrum Analysis

As described earlier Response history analysis (RHA) provides structural response $r(t)$ as a function of time, when structural designs are usaually based on peak values of forces and deformations over the duration of the earthquake induced response. This method is considered ideal for SDF systems but when it comes to MDF systems the results in the sense that it is not identical to the RHA results, never the less the estimate obtained is accurate enough for structural design application.

From the response spectrum the peak value of r_{no} can be obtained from the pseudo-acceleration spectrum as its ordinate $A(T_n, \zeta_n)$ denoted as A_n. Therefore,

$$r_{no} = r_n^{st} A_n \tag{4-42}$$

The modal responses $r_n(t)$ attain their peaks at different time instants and the combined response $r(t)$ attains its peak at yet a different instant. Approximations must be used to combine the peak modal responses r_{no} since no information is available when theses peak modal values occur. Three different methods are used:

- Absolute sum (ABSSUM)
- Square-root-of-sum-of-squares (SRSS)
- Complete quadratic combination (CQC)

ABSSUM method assumes that the modal peaks occurs at the same time and ignores their algebraic sign therefore providing an upper bound to the peak value of the total response. This method is usually considered too conservative. SRSS, Eq. ((4-43), on the other hand provides excellent response estimate for structures with well-separated natural frequencies. The square root is taken of the sum of each peak modal response squared, to achieve an estimate of the peak total response.

$$r_o \cong \left(\sum_{n=1}^{N} r_{no}^2 \right)^{\frac{1}{2}} \tag{4-43}$$

The CQC method is considered in a wider class of structures as it overcomes the limitations of the SRSS method (Chopra, 2007).

5 Earthquake response analysis of wind turbine

5.1 Earthquake seismic information

Over the course of the last 24 years the monitoring system has recorded a large amount of earthquake induced acceleration records. The focus of this study is on the three large earthquakes recorded on June 17th 2000, June 21st 2000 and May 29th 2008. These three events have been discussed briefly in chapter 3. The key earthquake parameters are listed in Table 5-1.The locations of the earthquake epicentres are shown in Figure 3-9.

Table 5-1. The earthquakes chosen for further analysis

Date and time	Number of Stations	Magnitude	Latitude	Longitude
		M_w	Degrees	Degrees
17.6.2000	24	6,5	63,97	-20,36
21.6.2000	24	6,4	63,97	-20,71
29.5.2008	8	6,3	64,01	-21,01

Time series of the recorded ground motion among other information's were gathered from the European Strong-Motion Database website (Ambraseys, et al., 2004). An example of recorded earthquake ground acceleration time series are shown in Figure 5-1. The time series are recorded during the largest earthquake, occurring June 17, 2000. Before applying the time series for analysis, the actual strong motion part of the recording is selected as shown in Figure 5-1 (bottom).

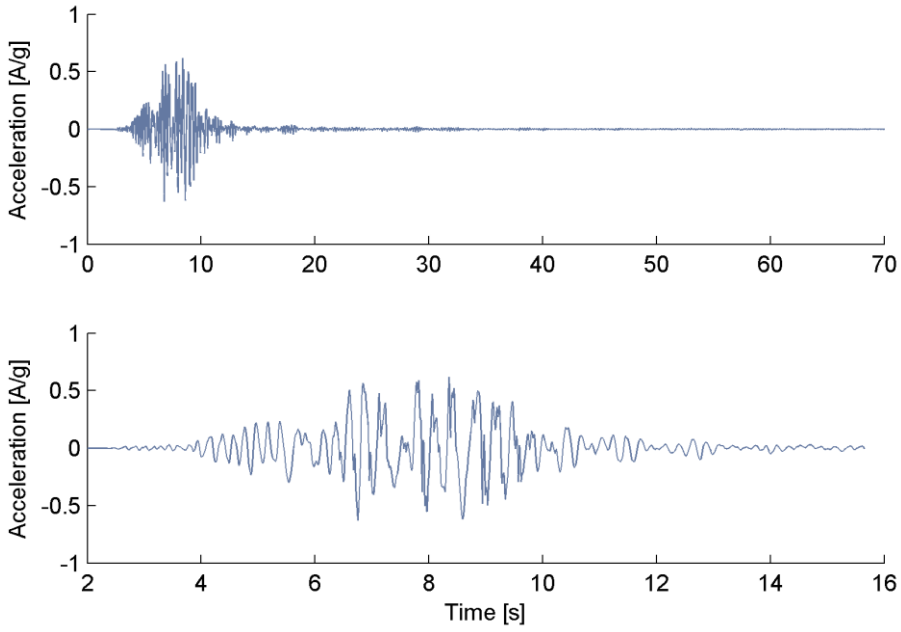

Figure 5-1. Earthquake response time series of June 17, 2000.
Acceleration Time-series from database (top),
Acceleration Time-series used in analysis (bottom).

5.2 The wind turbine

In December 2012, Landsvirkjun erected two wind turbines, as a part of research and development project on the advantageous of wind power in Iceland, at Búrfell Power Station in south Iceland. From Enercon Germany, the two turbines have a total of 2 MW power installed expected to generate up to 5.4 GWh per year. The mast is 55 meters high and each blade measures 22 meters in length reaching 77 meters at their highest point (Landsvirkjun, 2013).

Table 5-2. Main parameters of wind turbine

Technical specifications E-44	
Rated power:	900 kW
Rotor diameter:	44 m
Hub height:	45 m / 55 m
Mass of rotor	15.000 kg
Mass of nacelle	22.000 kg
Mass of tower	52.050 kg

The tower is a tapered hollow steel tube made of sheets with a base diameter of 3.3 meters and a wall thickness of 0.024 meters, and a top diameter of 1.3 meters with a wall thickness of 0.016 meters. The tower is constructed in three sections, two around 17 meters high and third one around 19 meters high. Steel density is considered to be 7850 kg/m^3.

Figure 5-2. Image of a 900 kW Wind Turbine at Burfell hydropower station.
Manufactured by Enercon (Landsvirkjun, 2013).

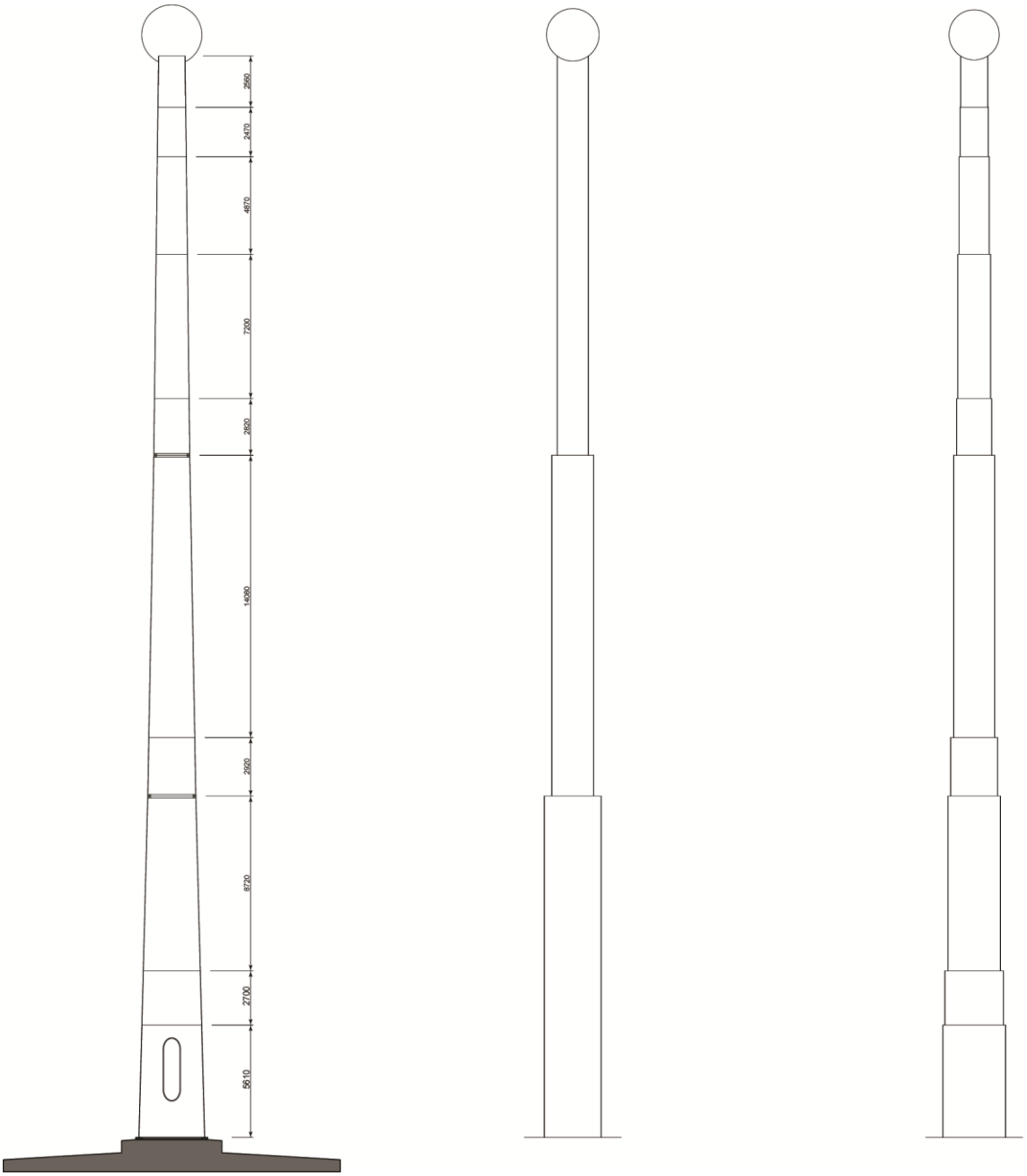

Figure 5-3. Elevation of Enercon Wind Turbine Tower. Specification from manufacture (left).
Illustration of a 3 element model analized in Matlab (middle). Illustration of a 10 element model analized in Matlab (right)

5.3 Modelling

Early investigations (Bazeos, et al., 2002); (Lavassas, et al., 2003) of earthquake loading focused on tower loading using models that lump the nacelle and rotor as a point mass. These were incapable of considering the simultaneous combination of seismic and wind loads. Gradually, interest shifted from these simple models to more refined models as described in section 2.2. However this study is a preliminary research on earthquake analysis on wind turbines in Iceland, therefore only effects of seismic forces will be analysed. In the following subchapters the analysis process is explained where the three element model will be used as a calculation reference, followed by analysis results in chapter 6.

To estimate the seismic action demand on the wind turbine, different models were used. Properties for equivalent beam elements were developed for the tower using engineering drawings and specifications in Table 5-2. A three-element model was made, where each element represented the three sections that make up the tower and a ten-element model that takes into account the wall thickness dividing each section into two or three parts, Figure 5-3. The mass of each element is divided between adjacent nodes and the mass of the rotor and nacelle is placed as a point mass on top of the tower. Same procedure applies for models regardless of their element count.

5.3.1 Matlab modelling workflow

The main analysis program (*Run_external.m*) imports the tower specifications from external text files using a subroutine (*Import_Data.m*). Information of the tower elements like height, mass, modulus and inertia are gathered for further calculations. An overview of the workflow can be seen in Figure 5-4. In the following sections, an overview on the analysis will be provided through a detailed presentation of results for the 3-element model using an example ground motion timehistory.

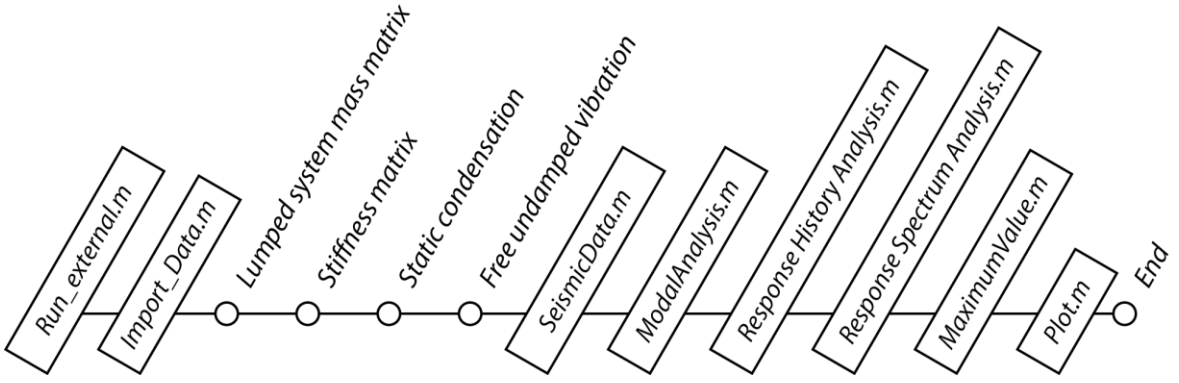

Figure 5-4. The workflow of the main analysis program (Run_external.m).

Lumped system mass matrix

The mass is pre-calculated using equation (5-1), for a given cross sectional area and height of element assuming a steel density of 7850 kg/m^3.

$$W = A \cdot H_{el} \cdot \rho \ [kg] \tag{5-1}$$

After importing the mass to the main file the mass is distributed to the end nodes of each element. Since the tower is tapered $5/8$ of the mass was accociated to the first (lower) node leaving 3/8 of the mass to the second node. The distribution throughout the tower is as follows:

$$M_{1,2} = \frac{3}{8} \cdot M_1 + \frac{5}{8} \cdot M_2 \quad M_{N-1,2} = \frac{3}{8} \cdot M_{N-1} + \frac{5}{8} \cdot M_N \quad M_{N,2} = M_{N,2} + M_{R+N}$$

Where $M_{1,2}$, is the mass of node 2 in the ground element, $and\ M_{N,2}$ is the mass of the top element along with M_{R+N} mass of the rotor and nacelle.

$$M_{tower} = \begin{bmatrix} M_{1,2} & 0 & 0 \\ 0 & M_{2,2} & 0 \\ 0 & 0 & M_{N,2} + M_{R+N} \end{bmatrix} \tag{5-2}$$

For the 3-element model the diagonal mass matrix is:

$$M_{tower} = \begin{bmatrix} 18683 & 0 & 0 \\ 0 & 13210 & 0 \\ 0 & 0 & 41575 \end{bmatrix} kg \tag{5-3}$$

Element stiffness

To calculate the tower stiffness the moment of inertia is calculated with equation (5-4, for each element. Since the tower is tapered the model is simplified by averaging the outer diameter D and inner diameter d of each section of the tower to maintain a constant cross section see Figure 5-2.

$$I = \frac{\pi}{64} \cdot [D^4 - d^4] \ [m^4] \tag{5-4}$$

The tower is considered as a beam element of length L and flexural rigidity EI. The elements stiffness matrix can be described as follows:

$$k_e = \frac{EI}{L^3} \begin{bmatrix} 12 & 6L & -12 & 6L \\ 6L & 4L^2 & -6L & 2L^2 \\ -12 & -6L & 12 & -6L \\ 6L & 2L^2 & -6L & 4L^2 \end{bmatrix} \tag{5-5}$$

Where the first and third term is related to deflection at joint 1 and 2 respectively and the second and forth terms relate to rotational displacement of joint 1 and 2. The element stiffness matrix is then combined at the joint intersection creating the system stiffness matrix K.

The base point is considered as a fixed point, therefore the first two lines and columns of the system stiffness matrix K are removed. Finally, since seismic load is the only external load affecting the system only the displacement terms of the stiffness matrix is needed, therefore a static condensation of the stiffness matrix is performed as described in section 0. The final condensed stiffness matrix is as follows:

$$\widehat{\boldsymbol{k}}_{\boldsymbol{tt}} = \boldsymbol{k}_{\boldsymbol{tt}} - \boldsymbol{k}_{\boldsymbol{0t}}^{-\boldsymbol{1}} \boldsymbol{k}_{\boldsymbol{00}}^{-\boldsymbol{1}} \boldsymbol{k}_{\boldsymbol{0t}} \tag{5-6}$$

The total stiffness matrix for a 3-element is an $[8\ x\ 8]$ matrix but reduces to a $[3\ x\ 3]$ matrix after the static condensation and implementation of boundary conditions.

The final condensed stiffness matrix for the 3-element model is.

$$\widehat{\boldsymbol{k}}_{\boldsymbol{tt}} = \begin{bmatrix} 7.133 & -2.490 & 0.348 \\ -2.490 & 1.665 & -0.392 \\ 0.348 & -0.392 & 0.1483 \end{bmatrix} \cdot 10^7\ Nm \tag{5-7}$$

Free undamped vibration

Using the condensed stiffness matrix $\hat{k}_{tt}$ and the diagonal mass matrix M_{tower} the natural periods and corresponding mode shapes are calculated with the built in function in Matlab.

$$[\phi, \omega^2] = eig(\hat{k}_{tt}, M_e) \tag{5-8}$$

Using the output data from the built in function the natural frequencies, and natural periods are calculated as described in section 4.2.1.

For the 3-element model the natural frequencies are:

$$\omega_n = \begin{bmatrix} 3.02 \\ 22.83 \\ 67.70 \end{bmatrix} \qquad f_n = \begin{bmatrix} 0.48 \\ 3.63 \\ 10.77 \end{bmatrix} \qquad T_n = \begin{bmatrix} 2.08 \\ 0.275 \\ 0.093 \end{bmatrix}$$

The corresponding mode shapes are:

$$\phi_1 = \begin{bmatrix} 0.0721 \\ 0.3459 \\ 1.0 \end{bmatrix} \qquad \phi_2 = \begin{bmatrix} 0.411 \\ 1.0 \\ -0.123 \end{bmatrix} \qquad \phi_3 = \begin{bmatrix} 1.0 \\ -0.570 \\ 0.030 \end{bmatrix}$$

The natural frequencies and mode shapes for the more complex models are summarized in section 6.1.

Selecting seismic data

As stated in section 3.2.3, the data used in this paper is received from ISESD project (Internet-Site for European Strong-Motion Data). The subroutine *SeismicData.m* is used to select between three seismic events and import the corresponding ground motion data. The function *Cor_In.m*, also available from ISESD, reads the cor-files from the database and outputs the sample size, sample rate,

acceleration', velocity' and displacement time history for the ground motion. The subroutine is called as: *[ns,tme,acc,vel,dis]=Cor_In(pathName,corData{i});*

After importing the data the relevant earthquake motion is picked out from the data files that include pre- and post event data mainly containing environmental noise. A 0,5 second section preceding the earthquake motion is selected and the maximum acceleration within that data is evaluated as an indication of the general noise level. The starting point of the reduced data is chosen as the point that is 0.5 seconds before the acceleration reaches 3 times the noise level. The total duration of all records was set to 20 seconds, see Figure 5-1 (bottom).

The subroutine *Location.m* is used to associate fault distance, epicentre distance and station name to the corresponding acceleration data.

Modal analysis

Using the method presented in section 4.2.2 the following modal parameters are evaluated for the 3-element model.

$$L_n^h = \begin{bmatrix} 4{,}749 \\ 1{,}577 \\ 1{,}241 \end{bmatrix} \cdot 10^4 \quad M_n = \begin{bmatrix} 4{,}325 \\ 1{,}7 \\ 2{,}301 \end{bmatrix} \cdot 10^4 \quad \Gamma_n = \begin{bmatrix} 1.098 \\ 0.927 \\ 0.539 \end{bmatrix}$$

The spatial distribution calculation for mode 1 of the 3-element model is

$$s_1 = 1.098 \cdot \begin{bmatrix} 18683 & 0 & 0 \\ 0 & 13210 & 0 \\ 0 & 0 & 41575 \end{bmatrix} \cdot \begin{bmatrix} 0.0721 \\ 0.3459 \\ 1.0 \end{bmatrix} = \begin{bmatrix} 0{,}148 \\ 0{,}502 \\ 4{,}565 \end{bmatrix} \cdot 10^4$$

The following matrix lists the complete ***s***-matrix for the 3-element model.

$$s_n = \begin{bmatrix} 0{,}148 & 0{,}713 & 1.007 \\ 0.502 & 1{,}225 & -0.406 \\ 4{,}565 & -0.475 & 0.068 \end{bmatrix} \cdot 10^4$$

The modal static response V_i is evaluated as:

$$V_n = \begin{bmatrix} 5{,}214 & 1{,}463 & 0{,}669 \\ 5{,}066 & 0{,}750 & -0{,}338 \\ 4{,}565 & -0{,}475 & 0{,}068 \end{bmatrix} \cdot 10^4$$

The modal static response M_i is evaluated as:

$$M_n = \begin{bmatrix} 2{,}659 & 0{,}282 & 0{,}070 \\ 1{,}771 & 0{,}033 & -0{,}044 \\ 0{,}909 & -0{,}095 & 0{,}013 \end{bmatrix} \cdot 10^6$$

Response History Analysis

Time analysis was performed using the subroutine *Response_History_Analysis.m*, see

Appendix B, which again uses a Newmark integration scheme formulated in the subroutine *NewmarkL.m.*

The time history of displacement response, base shear and base moment for the 3-element model is shown in Figure 5-5 for the ground acceleration recorded at Kaldárholt on June 17, 2000.

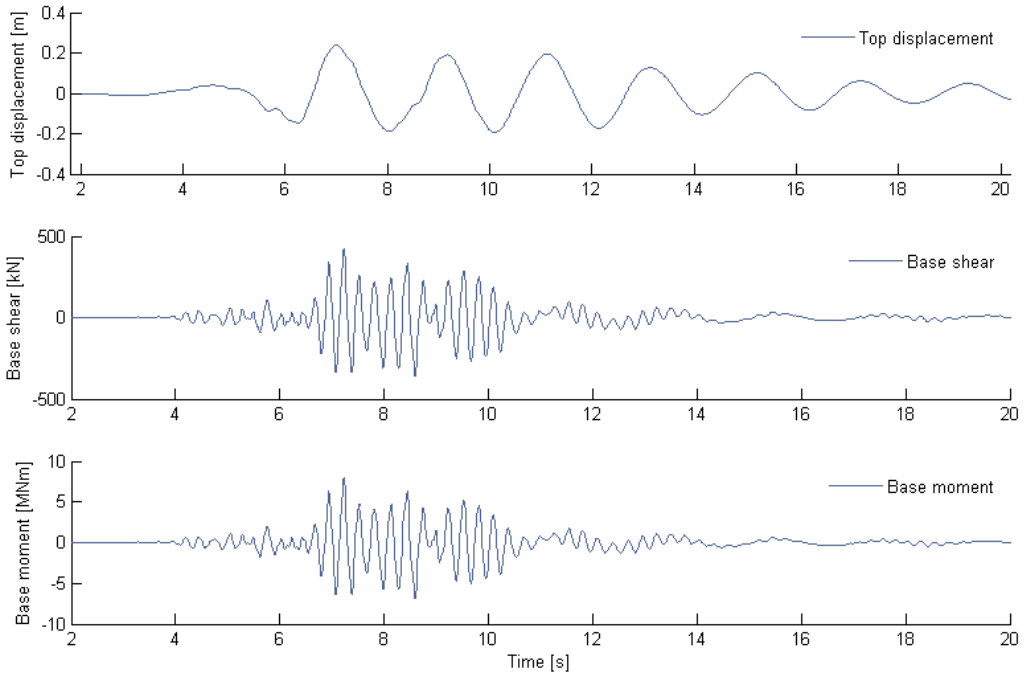

Figure 5-5. Time series at Kaldárholt on June 17th 2000.

Finally the total response is calculated using Eq. (4-27)

For the shear forces eq. (4-27) becomes:

$$V(t) = \sum_{n=1}^{N} V_n(t) = \sum_{n=1}^{N} V_i A_n(t)$$

And for moment forces:

$$M(t) = \sum_{n=1}^{N} M_n(t) = \sum_{n=1}^{N} M_i A_n(t)$$

Story shear force and story moment force at Kaldarholt is,

$$V = \begin{bmatrix} 138 & 143 \\ 187 & 179 \\ 425 & 299 \end{bmatrix} kN \qquad M = \begin{bmatrix} 2{,}7 & 2{,}8 \\ 1{,}7 & 3{,}8 \\ 8{,}6 & 8{,}5 \end{bmatrix} MN\text{m}$$

Response Spectrum Analysis

Response spectrum analysis was performed using the subroutine *Response_Spectrum_Analysis.m*, see

Appendix B, which again uses a Newmark integration scheme formulated in the subroutine *NewmarkL.m.* The Eurocode type 1 spectrum, gathered from *EuroSpectrum.m*, is plotted alongside the response spectrum as a guideline.

The Response spectrum acceleration for the 3-element model is shown in Figure 5-6 for the ground acceleration recorded at Kaldárholt on June 17, 2000.

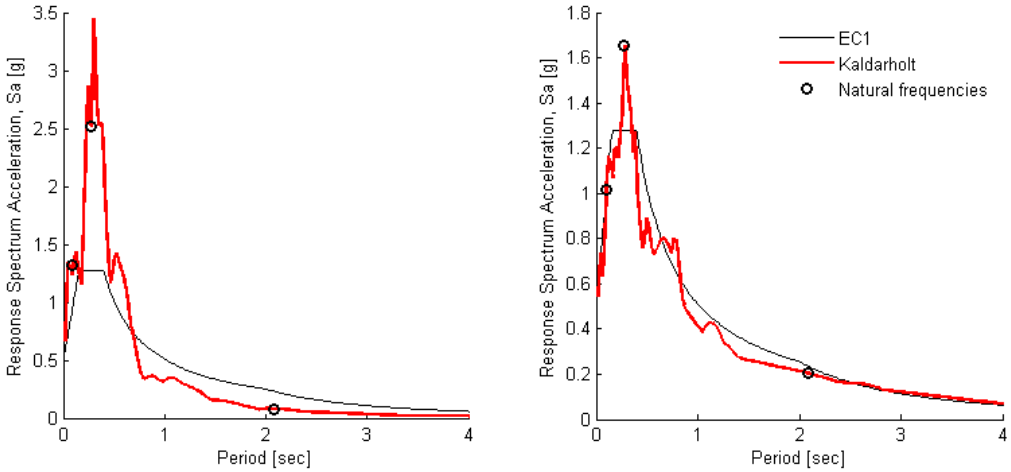

Figure 5-6. Response spectrum analysis at Kaldárholt on June 17th 2000.

The total response is calculated using Eq.

For the shear and moment forces eq. (4-42) becomes:

$$V = V_i A_n \qquad M = M_i A_n$$

Approximating the peak modal responses using SRSS gives:

Story shear force and story moment force at Kaldarholt is,

$$V = \begin{bmatrix} 124 & 119 \\ 196 & 162 \\ 375 & 268 \end{bmatrix} kN \qquad M = \begin{bmatrix} 2{,}5 & 2{,}4 \\ 1{,}8 & 3{,}6 \\ 7{,}4 & 7{,}0 \end{bmatrix} MN\text{m}$$

Plot

Finally the *plot.m* subroutine plots out the relavant plots seen in this study.

5.3.2 Import from SAP

Using the information from SAP the same subroutines described before are used except instead of using Run_External.m another subroutine, *Run_SAP.m*, is used. This subroutine imports the element mass, mode shapes and participation factor among others variables needed to run the modal analysis, RHA and RSA.

5.3.3 SAP model

Acceleration, Periods and Spectral acceleration data corresponding to the site where the highest seismic effect where calculated were exported as a text file to be used in SAP2000. The same TH and SA analysis were made and the results compared.

6 Structural modelling and earthquake analysis

6.1 Modal analysis

As discussed and demonstrated in Chapter 5, modal analysis were done for the three different models developed. The resulting natural frequencies are listed in Table 6-1 along with the effective mass associated with each mode of vibration. The table also shows the natural frequencies evaluated for the 900 kW wind turbine studied by Prowell et al. (2010). The corresponding mode shapes for the first three modes are shown in Figures 6-1, 6-2 and 6-3.

Table 6-1. Natural frequencies for three Matlab models and two SAP models, along with their effective modal mass

Lateral Modes	**3 Element model**	**Effective Modal mass**	**10 Element model**	**Effective Modal mass**	**3D SAP model**	**Effective Modal mass**	**3D SAP model with eccentricity**	**Effective Modal mass**	**900 kW Reference Model**
	Frequency (Hz)	%	Frequency (Hz)	%	Frequency (Hz)	%		%	Frequency (Hz)
1	0,48	71	0,48	62	0,47	63	0,47	63	0.56
2	3,63	91	3,90	78	3,72	78	3,51	76	3,96
3	10,77	100	10,56	88	10,37	88	8,74	84	-
4	-	-	21,57	89	18,4	88	18,09	89	-
5	-	-	43,65	99	48,25	90	30,13	90	-
6	-	-	62,65	99	53,06	99	38,59	99	-
7	-	-	99,59	99	78,97	99	68,65	99	-
8	-	-	121,65	99	88,43	99	81,38	99	-

Figure 6-1. Mode shapes for Mode 1.
3 Element Model (left), 10 Element Model (middle) and SAP Model (right).

Figure 6-2. Mode shapes for Mode 2.
3 Element Model (left), 10 Element Model (middle) and SAP Model (right).

Figure 6-3. Mode shapes for Mode 3.
3 Element Model (left), 10 Element Model (middle) and SAP Model (right).

6.2 Response Analysis

Figures 6-4, 6-5 and 6-6, shows the tower displacements, shear forces and overturning moment as a function of tower height, for the three locations and events that gave the largest response. The three locations and events are: Flagbjarnarholt during the June 17, 2000 earthquake; Þjórsárbrú during the June 21, 2000 earthquake and Hveragerði during the May 29, 2008 event.

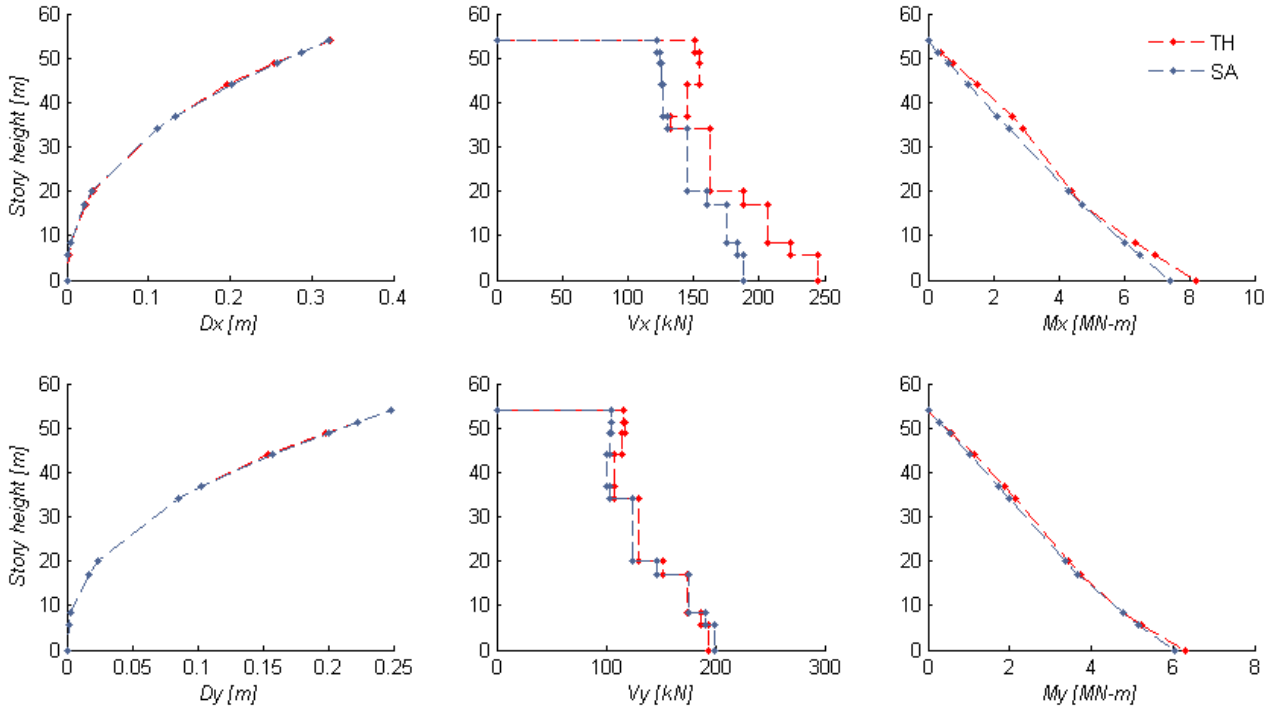

Figure 6-4. Maximum displacement and reaction forces at Flagbjarnarholt in June 17th 2000.
East direction (left) and south direction (right)

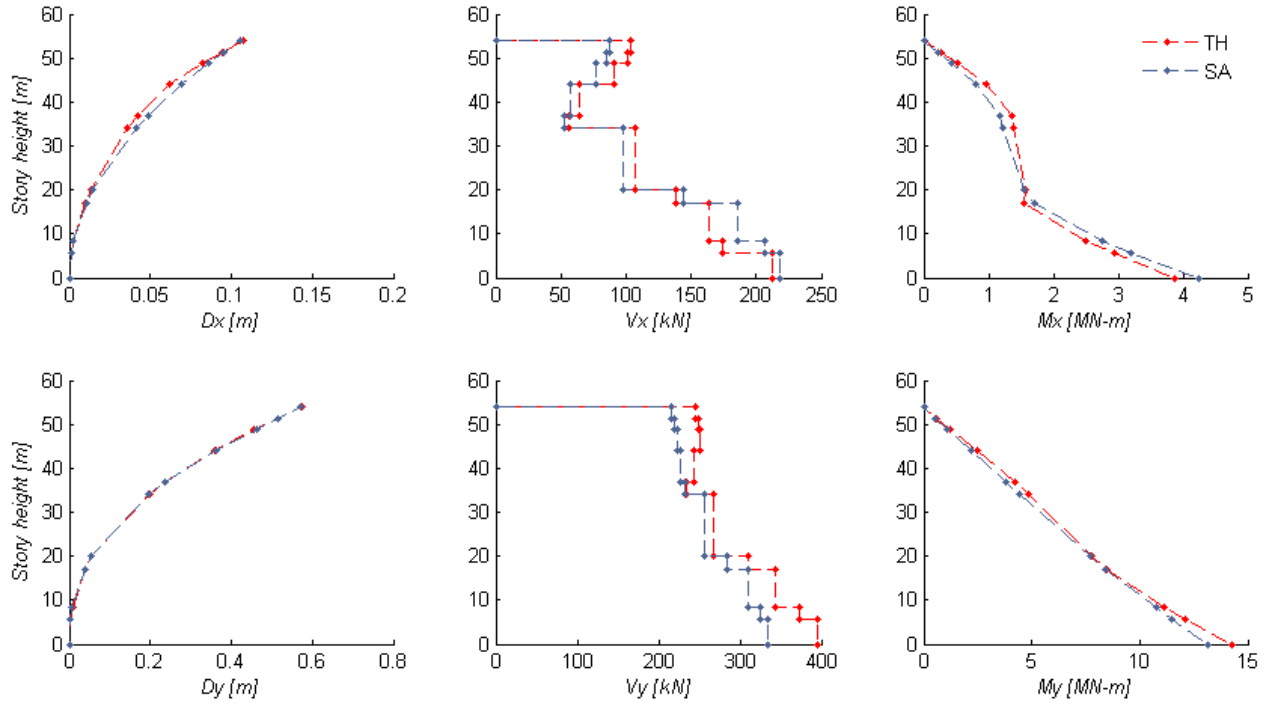

Figure 6-5. Maximum displacement and reaction forces at Þjórárbrú in June 21th 2000.
West direction (left) and North direction (right).

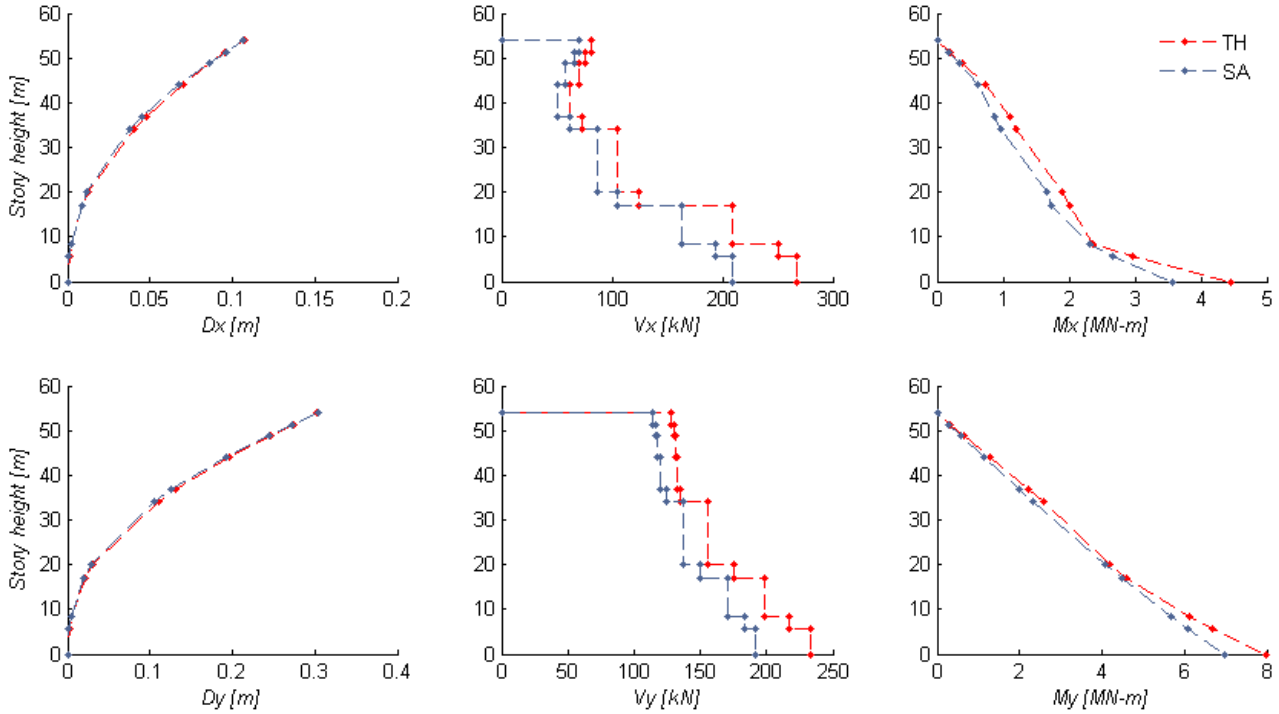

Figure 6-6. Maximum displacement and reaction forces at Hveragerði in May 29th 2008.
North direction (left) and West direction (right).

Figures 6-7, 6-9 and 6-9, show the base moment time series at the three locations that gave the highest reaction forces during each of the three events considered.

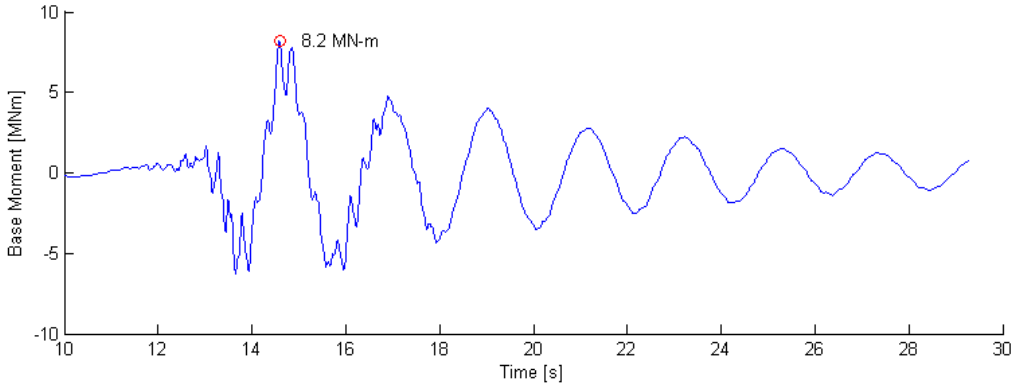

Figure 6-7. Base Moment at Flagbjarnarholt in June 17th 2000.
East direction (left) and south direction (right)

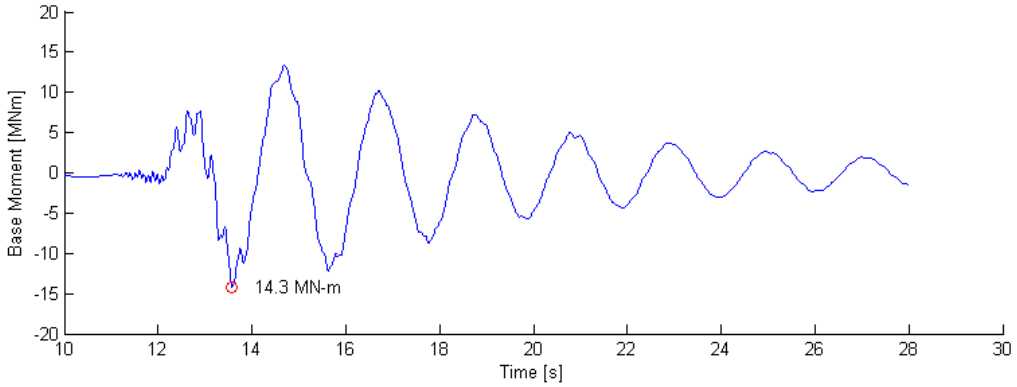

Figure 6-8. Base Moment at Þjórsárbrú in June 21th 2000.
West direction (left) and North direction (right).

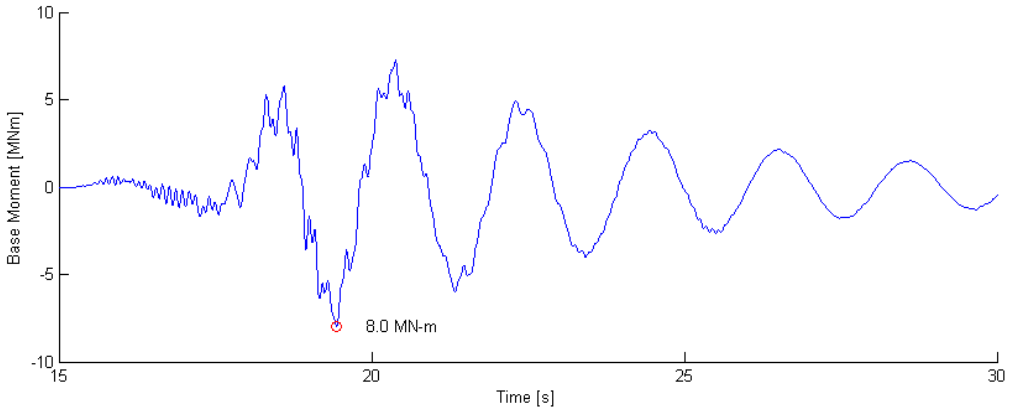

Figure 6-9. Base Moment at Hveragerði – Retirement house in May 29th 2000.
North direction (left) and West direction (right).

Figures 6-10, 6-11 and 6-12, show the base shear time series at the three locations that gave the highest reaction forces during each of the three events considered.

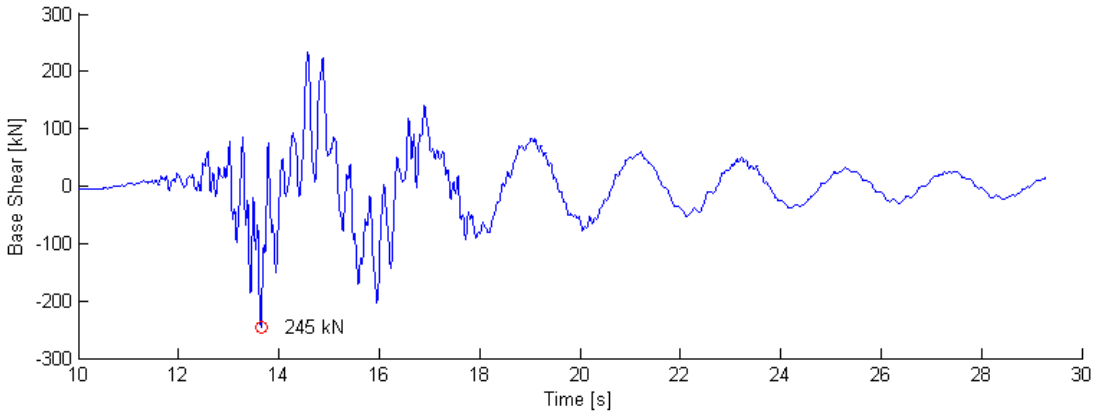

Figure 6-10. Base Shear at Flagbjarnarholt in June 17th 2000.
East direction (left) and south direction (right)

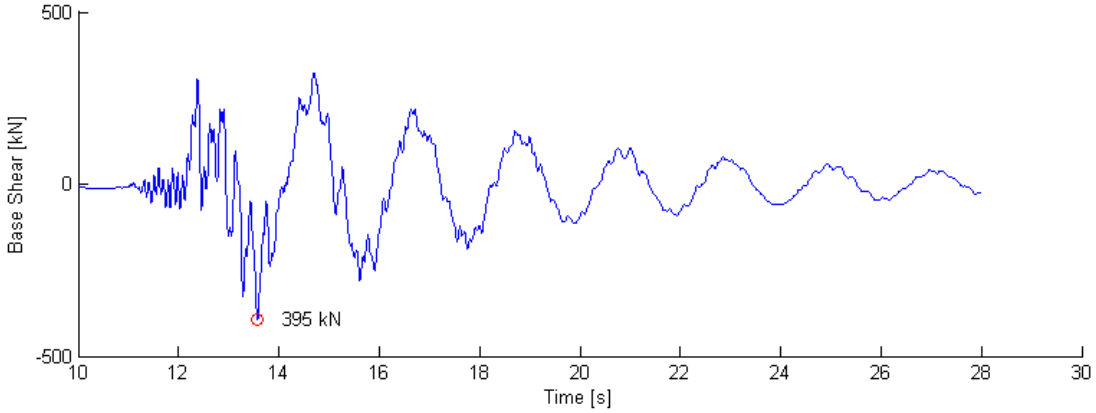

Figure 6-11. Base Shear at Þjórsárbrú in June 21th 2000.
West direction (left) and North direction (right).

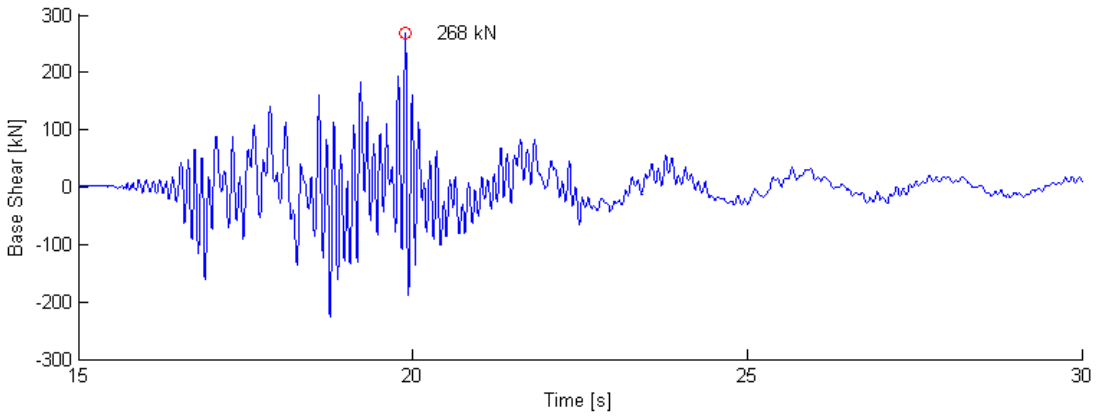

Figure 6-12. Base Shear at Hveragerði – Retirement house in May 29th 2000.
North direction (left) and West direction (right).

Figures 6-13, 6-14 and 6-15, show the response spectrum at the three locations that gave the highest reaction forces during each of the three events considered. The respective response spectra are compared with the Eurocode spectra (type 1). The natural frequencies of the tower are also plotted to show how they relate to the spectral accelerations.

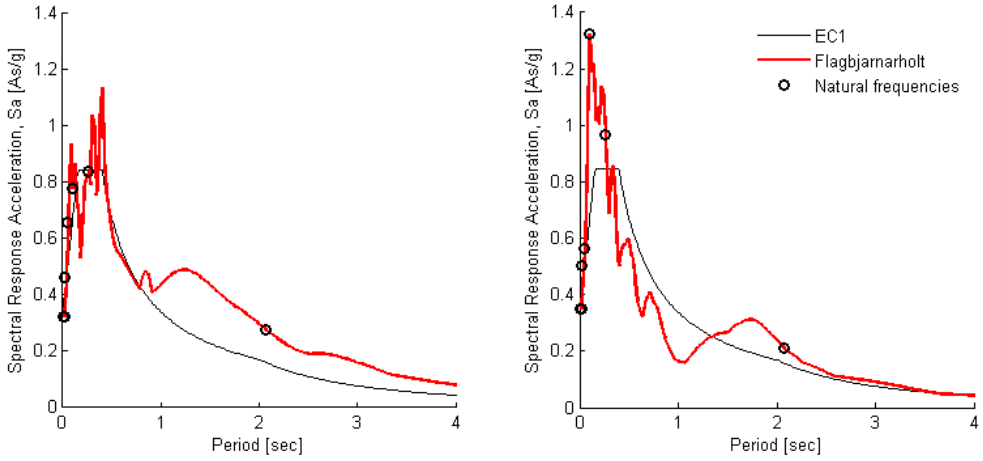

Figure 6-13. Response Spectrum at Flagbjarnarholt, June 17th 2000.
East direction (left) and South direction (right).

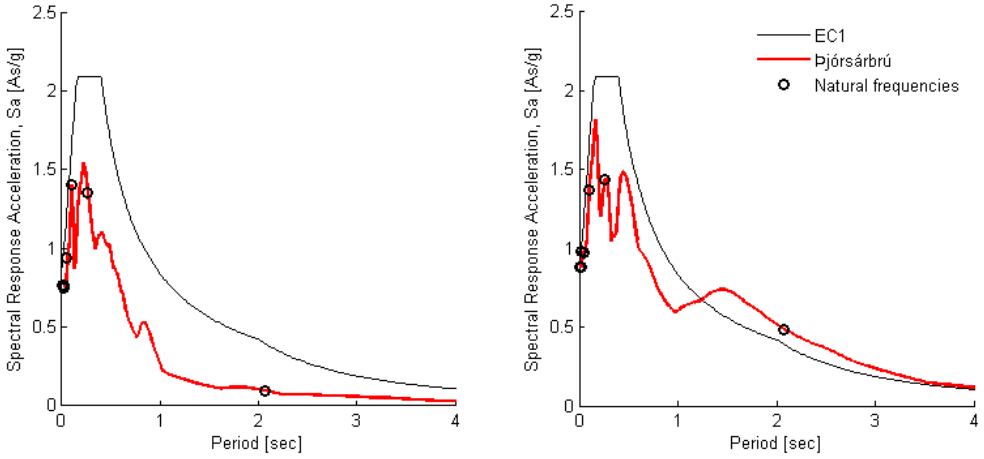

Figure 6-14. Response Spectrum at Þjórsárbrú, June 21th 2000.
West direction (left) and North direction (right).

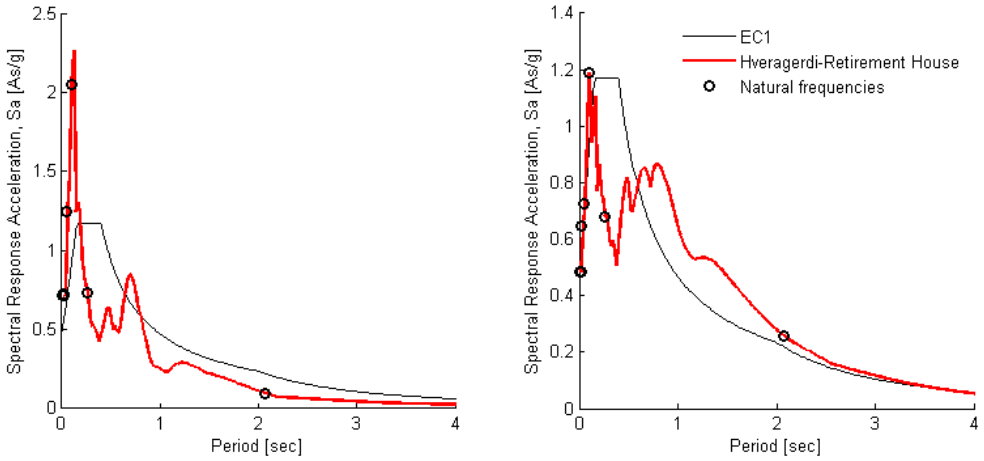

Figure 6-15. Response Spectrum at Hveragerði, May 29th 2000.
North direction (left) and West direction (right).

Table 6-2, summarizes the top displacement, base shear and base moment of a 3 element model for ground motion recordings from the earthquake on June 17th 2000.

Table 6-2. Summary of Seismic response of 3 element model for ground motion recordings from June 17th 2000

Station	**Distance to source**	**PGA**	D_{peak}	$V_{b_{peak}}$		$M_{b_{peak}}$		***Direction***	
				TH	***SA***	***TH***	***SA***	***TH***	***SA***
	$[km]$	$[g]$	$[m]$	$[kN]$	$[kN]$	$[MNm]$	$[MNm]$	[X , Y]	[X , Y]
Kaldarholt	6	0,62	0,241	426	375	8,6	7,4	X	X
Flagbjarnarholt	4	0,34	0,318	240	185	8,2	7,4	X	X
Hella	10	0,39	0,232	219	182	7,1	5,8	Y	Y
Þjórsárbrú	14	0,37	0,140	212	221	4,9	5,1	Y	Y
Minni-Núpur	10	0,16	0,105	71	67	2,5	2,5	X	X
Sólheimar	15	0,40	0,092	118	108	2,1	2,4	X	X
Selfoss - Hospital	31	0,07	0,072	47	38	1,6	1,6	Y	Y
Hveragerði – Retirem.	41	0,11	0,065	49	37	1,5	1,5	X	X
Selfoss - City Hall	32	0,07	0,064	41	37	1,5	1,5	X	X
Þorlákshöfn	51	0,05	0,057	30	30	1,2	1,3	X	X
Búrfell - Hydro	26	0,08	0,046	45	41	1,2	1,2	X	X
Hveragerði - Church	41	0,11	0,050	38	35	1,2	1,2	X	X
Sigöldu - dam	63	0,04	0,045	19	23	1,0	1,0	Y	Y
Ljósafoss - Hydro	33	0,07	0,031	29	28	0,8	0,8	X	X
Írafoss - Hydro	33	0,04	0,028	17	18	0,6	0,7	X	X
Hrauneyjafoss - Hydro	58	0,02	0,025	10	12	0,5	0,6	Y	Y
Sultartangi - Hydro	39	0,04	0,023	13	15	0,5	0,5	Y	Y
Sultatangi - dam	42	0,02	0,021	13	15	0,5	0,5	X	X
Reykjavík University	79	0,03	0,010	12	13	0,3	0,3	Y	Y
Reykjavík - Heiðmörk	69	0,04	0,014	13	12	0,3	0,3	Y	Y
Sigöldu - Hydro	62	0,01	0,011	6	6	0,2	0,2	X	X
Reykjavík - Foldaskóli	71	0,01	0,005	7	6	0,2	0,2	Y	Y
Reykjavík - Hús Versl.	77	0,02	0,007	6	6	0,2	0,2	X	X
Blöndu - dam	138	0,00	0,001	1	1	0,0	0,0	X	Y

Table 6-3, summarizes the top displacement, base shear and base moment of a 3 element model for ground motion recordings from the earthquake on June 21th 2000.

Table 6-3. Summary of Seismic response of 3 element model for ground motion recordings from June 21st 2000

Station	**Distance to source**	**PGA**	D_{peak}	$V_{b_{peak}}$		$M_{b_{peak}}$		***Direction***	
				TH	***SA***	***TH***	***SA***	***TH***	***SA***
	$[km]$	$[g]$	$[m]$	$[kN]$	$[kN]$	$[MNm]$	$[MNm]$	[X , Y]	[X , Y]
Þjórsárbrú	3	0,84	0,571	407	333	15,5	13,2	Y	Y
Þjórsártún	3	0,57	0,535	317	273	12,7	12,0	Y	Y
Sólheimar	4	0,72	0,478	236	256	10,3	10,8	Y	Y
Kaldarholt	11	0,39	0,111	193	193	3,8	3,9	Y	X
Ljósafoss - Hydro	16	0,11	0,139	72	69	3,2	3,1	Y	Y
Írafoss - Hydro	16	0,10	0,127	62	63	2,9	2,9	Y	Y
Selfoss - Hospital	14	0,11	0,112	80	70	2,9	2,6	Y	Y
Hella	19	0,13	0,071	106	91	2,7	2,3	Y	Y
Selfoss - City Hall	15	0,13	0,097	84	72	2,7	2,4	X	X
Þorlákshöfn	35	0,08	0,057	71	64	1,9	1,7	X	X
Hveragerði – Retirem.	24	0,10	0,074	49	46	1,8	1,7	X	X
Hveragerði - Church	24	0,08	0,059	39	37	1,4	1,4	X	X
Flagbjarnarholt	22	0,04	0,058	43	34	1,4	1,3	X	X
Minni - Núpur	27	0,03	0,047	24	22	1,1	1,1	Y	Y
Búrfell - Hydro	43	0,03	0,032	16	17	0,7	0,7	X	X
Sigöldu - dam	79	0,01	0,023	10	11	0,5	0,5	Y	Y
Reykjavík - school	54	0,01	0,020	10	10	0,5	0,5	X	X
Hrauneyjafoss - Hydro	74	0,01	0,020	9	9	0,4	0,5	Y	Y
Reykjavík - Hús Versl.	60	0,02	0,017	9	9	0,4	0,4	X	X
Sigöldu - Hydro	79	0,01	0,018	8	8	0,4	0,4	X	X
Sultatangi - dam	58	0,01	0,017	9	8	0,4	0,4	X	X
Sultatangi - Hydro	55	0,02	0,017	8	8	0,4	0,4	X	X
Reykjavík - Heiðmörk	52	0,01	0,017	8	8	0,4	0,4	X	X
Blöndustífla	141	0,00	0,003	1	2	0,1	0,1	X	X

Table 6-4 summarizes the top displacement, base shear and base moment of a 3 element model for ground motion recordings from the earthquake on May 29th 2008

Table 6-4. Summary of Seismic response of 3 element model for ground motion recordings from May 29th 2008

Station	**Distance to source**	**PGA**	D_{peak}	$V_{b_{peak}}$		$M_{b_{peak}}$		$Direction$	
				TH	SA	TH	SA	TH	SA
	$[km]$	$[g]$	$[m]$	$[kN]$	$[kN]$	$[MNm]$	$[MNm]$	[X , Y]	[X , Y]
Hveragerði – Retirem.	3	0,66	0,300	238	181	7,2	6,9	Y	Y
Selfoss - Hospital	19	0,51	0,143	137	149	4,0	4,0	X	X
Selfoss - City Hall	18	0,31	0,138	146	122	3,6	3,4	Y	Y
Ljósafoss – Hydro	35	0,13	0,092	53	52	2,1	2,1	X	X
Hella	90	0,05	0,017	39	34	1,0	0,7	X	X
Þjórsárbrú	57	0,10	0,028	34	34	0,9	0,8	X	X
Reykjavík - Heiðmörk	72	0,04	0,024	11	13	0,5	0,5	X	X
Reykjavík - school	76	0,01	0,011	8	8	0,3	0,3	Y	Y

Table 6-5 summarizes the top displacement, base shear and base moment of a 10 element model for ground motion recordings from the earthquake on June 17th 2000.

Table 6-5. Summary of Seismic response of 10 element model for ground motion recordings from June 17th 2000

Station	**Distance to source**	**PGA**	D_{peak}	$V_{b_{peak}}$		$M_{b_{peak}}$		***Direction***	
				TH	***SA***	***TH***	***SA***	***TH***	***SA***
	$[km]$	$[g]$	$[m]$	$[kN]$	$[kN]$	$[MNm]$	$[MNm]$	[X , Y]	[X , Y]
Flagbjarnarholt	4	0,34	0,322	245	199	8,2	7,4	X	X
Kaldarholt	6	0,62	0,242	385	350	7,7	6,6	X	X
Hella	10	0,39	0,233	238	177	6,6	5,7	Y	Y
Þjórsárbrú	14	0,37	0,138	201	176	3,8	4,3	Y	Y
Minni-Núpur	10	0,16	0,105	95	79	2,9	2,6	X	X
Sólheimar	15	0,40	0,092	164	140	2,3	2,6	X	X
Selfoss - Hospital	31	0,07	0,072	45	38	1,6	1,6	Y	Y
Hveragerði – Retirem.	41	0,11	0,065	54	42	1,6	1,5	X	X
Selfoss - City Hall	32	0,07	0,064	44	38	1,5	1,5	X	X
Hveragerði - Church	41	0,11	0,050	44	40	1,2	1,2	X	X
Þorlákshöfn	51	0,05	0,058	32	31	1,2	1,3	X	X
Búrfell - Hydro	26	0,08	0,046	53	41	1,2	1,2	X	X
Sigöldu - dam	63	0,04	0,045	26	24	1,0	1,0	Y	Y
Ljósafoss - Hydro	33	0,07	0,032	27	26	0,7	0,8	X	X
Írafoss - Hydro	33	0,04	0,028	18	17	0,7	0,7	X	X
Hrauneyjafoss - Hydro	58	0,02	0,025	11	13	0,5	0,6	Y	Y
Sultartangi - Hydro	39	0,04	0,024	16	16	0,5	0,6	Y	Y
Sultatangi - dam	42	0,02	0,022	15	14	0,5	0,5	X	X
Reykjavík University	79	0,03	0,010	14	14	0,3	0,3	Y	Y
Reykjavík - Heiðmörk	69	0,04	0,014	13	12	0,3	0,3	X	X
Sigöldu - Hydro	62	0,01	0,011	6	6	0,2	0,3	X	X
Reykjavík - Hús Versl.	77	0,02	0,007	8	7	0,2	0,2	X	X
Reykjavík - Foldaskóli	71	0,01	0,005	7	6	0,2	0,2	Y	Y
Blöndu - dam	138	0,00	0,001	1	1	0,0	0,0	Y	Y

Table 6-6 summarizes the top displacement, base shear and base moment of a 10 element model for ground motion recordings from the earthquake on June 21th 2000.

Table 6-6. Summary of Seismic response of 10 element model for ground motion recordings from June 21st 2000

Station	**Distance to source**	**PGA**	D_{peak}	$V_{b_{peak}}$		$M_{b_{peak}}$		***Direction***	
				TH	***SA***	***TH***	***SA***	***TH***	***SA***
	$[km]$	$[g]$	$[m]$	$[kN]$	$[kN]$	$[MNm]$	$[MNm]$	[X , Y]	[X , Y]
Þjórsárbrú	3	0,84	0,574	395	334	14,3	13,1	Y	Y
Þjórsártún	3	0,57	0,539	308	276	12,6	12,1	Y	Y
Sólheimar	4	0,72	0,482	260	275	10,5	10,9	Y	Y
Kaldarholt	11	0,39	0,112	239	197	4,9	3,8	X	X
Ljósafoss - Hydro	16	0,11	0,137	70	66	3,1	3,1	Y	Y
Selfoss - Hospital	14	0,11	0,113	88	67	2,9	2,6	Y	Y
Írafoss - Hydro	16	0,10	0,126	61	62	2,8	2,8	Y	Y
Selfoss - City Hall	15	0,13	0,098	78	63	2,4	2,3	X	X
Hella	19	0,13	0,072	78	65	2,2	1,9	Y	Y
Hveragerði – Retirem.	24	0,10	0,074	49	47	1,7	1,7	X	X
Þorlákshöfn	35	0,08	0,057	54	49	1,5	1,5	X	X
Hveragerði - Church	24	0,08	0,059	37	37	1,4	1,4	X	X
Flagbjarnarholt	22	0,04	0,059	37	31	1,3	1,3	X	X
Minni - Núpur	27	0,03	0,047	25	22	1,0	1,0	Y	Y
Búrfell - Hydro	43	0,03	0,031	16	16	0,7	0,7	X	X
Sigöldu - dam	79	0,01	0,023	10	12	0,5	0,5	Y	Y
Reykjavík - school	54	0,01	0,019	10	9	0,4	0,4	X	X
Hrauneyjafoss - Hydro	74	0,01	0,020	9	9	0,4	0,4	Y	Y
Reykjavík - Hús Versl.	60	0,02	0,017	9	9	0,4	0,4	X	X
Sultatangi - dam	58	0,01	0,017	9	8	0,4	0,4	X	X
Sultatangi - Hydro	55	0,02	0,017	8	8	0,4	0,4	X	X
Reykjavík - Heiðmörk	52	0,01	0,017	8	8	0,4	0,4	X	X
Sigöldu - Hydro	79	0,01	0,017	8	8	0,4	0,4	X	X
Blöndustífla	141	0,00	0,003	2	2	0,1	0,1	X	X

Table 6-7 summarizes the top displacement, base shear and base moment of a 10 element model for ground motion recordings from the earthquake on May 29th 2008.

Table 6-7. Summary of Seismic response of 10 element model for ground motion recordings from May 29th 2008

Station	**Distance to source**	**PGA**	D_{peak}	$V_{b_{peak}}$		$M_{b_{peak}}$		$Direction$	
				TH	SA	TH	SA	TH	SA
	$[km]$	$[g]$	$[m]$	$[kN]$	$[kN]$	$[MNm]$	$[MNm]$	[X , Y]	[X , Y]
Hveragerði – Retirem.	3	0,66	0,303	268	210	8,0	7,0	Y	Y
Selfoss - Hospital	19	0,51	0,144	164	136	3,8	3,7	X	X
Selfoss - City Hall	18	0,31	0,139	185	124	3,7	3,3	Y	Y
Ljósafoss - Hydro	35	0,13	0,091	55	52	2,0	2,1	X	X
Þjórsárbrú	57	0,10	0,027	39	36	0,9	0,8	X	X
Hella	90	0,05	0,017	38	28	0,9	0,6	X	X
Reykjavík - Heiðmörk	72	0,04	0,024	12	13	0,5	0,5	X	X
Reykjavík - school	76	0,01	0,011	10	7	0,3	0,3	Y	Y

Table 6-8, summarizes the top displacement, base shear and base moment of the SAP model for ground motion recordings from the earthquake on June 17th 2000.

Table 6-8. Summary of Seismic response of SAP model for ground motion recordings from June 17th 2000

Station	**Distance to source**	**PGA**	D_{peak}	$V_{b_{peak}}$		$M_{b_{peak}}$		***Direction***	
				TH	***SA***	***TH***	***SA***	***TH***	***SA***
	$[km]$	$[g]$	$[m]$	$[kN]$	$[kN]$	$[MNm]$	$[MNm]$	[X , Y]	[X , Y]
Flagbjarnarholt	4	0,34	0,320	245	175	8,0	6,9	X	X
Kaldarholt	6	0,62	0,248	397	332	8,0	6,5	Y	X
Hella	10	0,39	0,236	208	170	6,5	5,4	Y	Y
Þjórsárbrú	14	0,37	0,155	196	194	4,1	4,8	Y	Y
Minni-Núpur	10	0,16	0,109	83	63	2,6	2,4	X	X
Sólheimar	15	0,40	0,095	154	133	2,2	2,5	X	X
Hveragerði – Retirem.	41	0,11	0,064	52	39	1,6	1,4	X	X
Selfoss - Hospital	31	0,07	0,074	46	37	1,6	1,6	Y	Y
Selfoss - City Hall	32	0,07	0,066	42	35	1,4	1,4	X	X
Þorlákshöfn	51	0,05	0,053	30	26	1,2	1,1	X	X
Hveragerði - Church	41	0,11	0,049	46	37	1,2	1,1	X	X
Búrfell - Hydro	26	0,08	0,047	45	36	1,1	1,1	X	X
Sigöldu - dam	63	0,04	0,046	21	21	1,0	1,0	Y	Y
Ljósafoss - Hydro	33	0,07	0,032	27	25	0,7	0,7	X	X
Írafoss - Hydro	33	0,04	0,028	18	17	0,6	0,6	X	X
Hrauneyjafoss - Hydro	58	0,02	0,025	10	11	0,5	0,5	Y	Y
Sultatangi - dam	42	0,02	0,020	13	13	0,4	0,5	X	X
Sultartangi - Hydro	39	0,04	0,022	15	14	0,4	0,5	Y	Y
Reykjavík University	79	0,03	0,011	14	13	0,3	0,3	Y	Y
Reykjavík - Heiðmörk	69	0,04	0,014	13	12	0,3	0,3	Y	Y
Sigöldu - Hydro	62	0,01	0,010	6	5	0,2	0,2	X	X
Reykjavík - Foldaskóli	71	0,01	0,006	7	5	0,2	0,1	Y	Y
Reykjavík - Hús Versl.	77	0,02	0,007	7	6	0,2	0,2	X	X
Blöndu - dam	138	0,00	0,001	1	1	0,0	0,0	Y	Y

Table 6-9, summarizes the top displacement, base shear and base moment of the SAP model for ground motion recordings from the earthquake on June 21st 2008.

Table 6-9. Summary of Seismic response of SAP model for ground motion recordings from June 21st 20008

Station	**Distance to source**	**PGA**	D_{peak}	$V_{b_{peak}}$		$M_{b_{peak}}$		***Direction***	
				TH	***SA***	***TH***	***SA***	***TH***	***SA***
	$[km]$	$[g]$	$[m]$	$[kN]$	$[kN]$	$[MNm]$	$[MNm]$	[X , Y]	[X , Y]
Þjórsárbrú	3	0,84	0,583	396	316	14,4	12,6	Y	Y
Þjórsártún	3	0,57	0,537	307	253	12,5	11,3	Y	Y
Sólheimar	4	0,72	0,479	246	258	9,8	10,2	Y	Y
Kaldarholt	11	0,39	0,112	180	171	4,0	3,4	X	X
Ljósafoss - Hydro	16	0,11	0,149	68	67	3,2	3,2	Y	Y
Selfoss - Hospital	14	0,11	0,114	88	65	2,9	2,5	Y	Y
Írafoss - Hydro	16	0,10	0,135	60	61	2,9	2,9	Y	Y
Selfoss - City Hall	15	0,13	0,096	87	63	2,5	2,2	X	X
Hella	19	0,13	0,071	89	77	2,4	2,0	Y	Y
Hveragerði – Retirem.	24	0,10	0,075	50	46	1,7	1,6	X	X
Þorlákshöfn	35	0,08	0,057	62	54	1,6	1,5	X	X
Hveragerði - Church	24	0,08	0,059	39	36	1,4	1,3	X	X
Flagbjarnarholt	22	0,04	0,054	39	29	1,3	1,1	X	X
Minni - Núpur	27	0,03	0,050	24	22	1,1	1,1	Y	Y
Búrfell - Hydro	43	0,03	0,035	16	17	0,8	0,7	X	X
Sigöldu - dam	79	0,01	0,024	10	11	0,5	0,5	Y	Y
Reykjavík - school	54	0,01	0,023	11	10	0,5	0,5	X	X
Hrauneyjafoss - Hydro	74	0,01	0,021	8	9	0,4	0,5	Y	Y
Reykjavík - Hús Versl.	60	0,02	0,019	9	9	0,4	0,4	X	X
Sultatangi - dam	58	0,01	0,019	9	8	0,4	0,4	X	X
Sigöldu - Hydro	79	0,01	0,020	8	8	0,4	0,4	X	X
Sultatangi - Hydro	55	0,02	0,018	8	8	0,4	0,4	X	X
Reykjavík - Heiðmörk	52	0,01	0,018	8	7	0,4	0,4	X	X
Blöndustífla	141	0,00	0,003	2	2	0,1	0,1	Y	Y

Table 6-10, summarizes the top displacement, base shear and base moment of the SAP model for ground motion recordings from the earthquake on May 29th 2008.

Table 6-10. Summary of Seismic response of SAP element model for ground motion recordings from May 29th 2008

Station	**Distance to source**	**PGA**	D_{peak}	$V_{b_{peak}}$		$M_{b_{peak}}$		$Direction$	
				TH	SA	TH	SA	TH	SA
	$[km]$	$[g]$	$[m]$	$[kN]$	$[kN]$	$[MNm]$	$[MNm]$	[X , Y]	[X , Y]
Hveragerði – Retirem.	3	0,66	0,301	238	196	7,3	6,5	Y	Y
Selfoss - Hospital	19	0,51	0,146	165	141	3,6	3,7	X	X
Selfoss - City Hall	18	0,31	0,141	185	119	3,4	3,2	Y	Y
Ljósafoss - Hydro	35	0,13	0,097	54	51	2,2	2,1	X	X
Hella	90	0,05	0,017	33	29	0,9	0,7	X	X
Þjórsárbrú	57	0,10	0,033	31	33	0,8	0,8	X	X
Reykjavík - Heiðmörk	72	0,04	0,026	12	13	0,6	0,5	X	X
Reykjavík - school	76	0,01	0,012	8	7	0,3	0,3	Y	X

In Figure 6-16, a comparison of the maximum base moment from all stations in the three events tested is plotted against their fault distance, is clear that the base moment reduces at a certain rate as the fault distance gets larger. In Figure 6-17, the base moment and base shear are plotter against the peak ground acceleration (PGA). As the PGA grows larger the base moment and base shear rise somewhat linearly to the PGA in the log-log scale depicted.

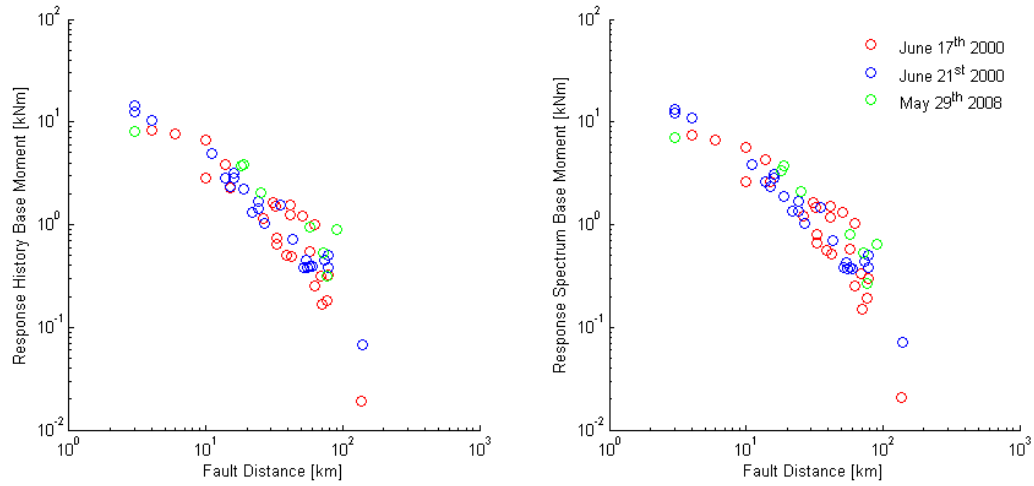

Figure 6-16. Base moment as a function of fault distance on June 17th and 21st 2000 and May 29th 2008 From Time History Analysis (left) and Response Spectrum Analysis (right)

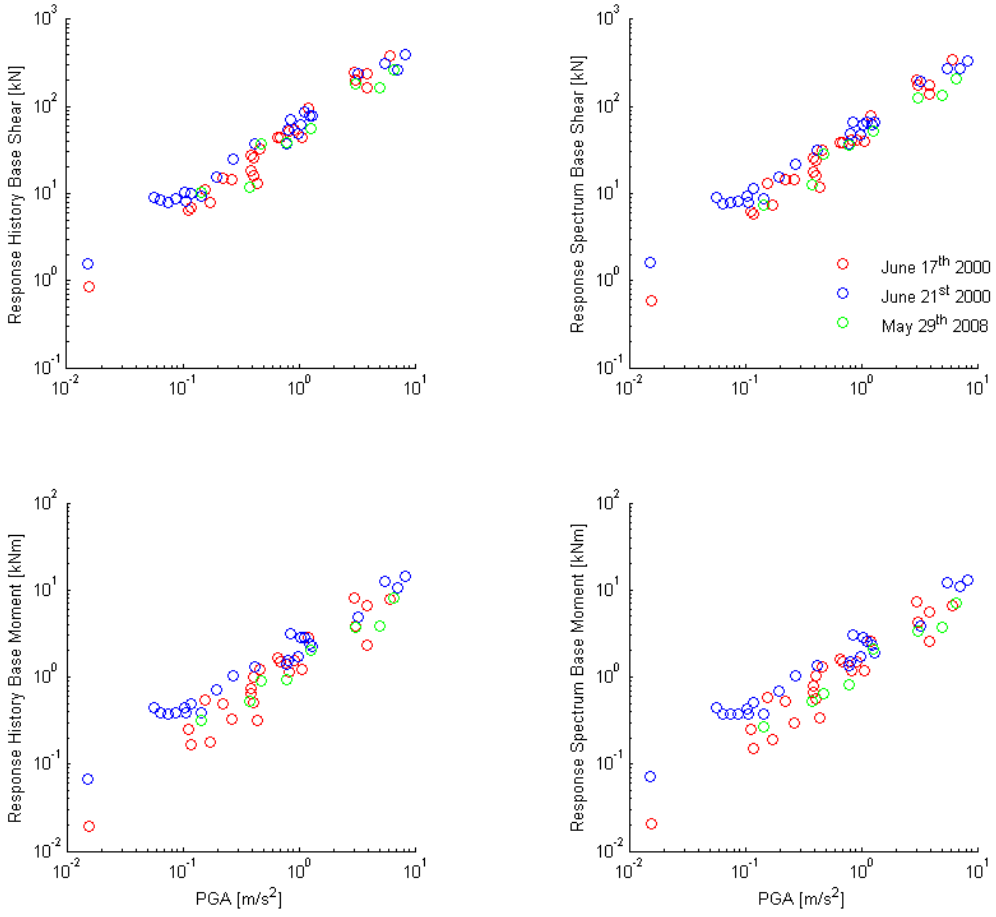

Figure 6-17. Base Shear and Base Moment as a function of PGA on June 17th and 21st 2000 and May 29th 2008 From Time History Analysis (left) and Response Spectrum Analysis (right)

6.3 Response Analysis in SAP

6.3.1 Setup

Given the same parameters used in Matlab a FE-model was created in SAP 2000. In Figure 6-18 the material properties is defined with the same material properties as used in Matlab routines, i.e. material density and modulus. Figure 6-20 displays one of eighteen cross sections that were combined to make up the tower. Finally a point mass of 37 tons was assigned to the top node.

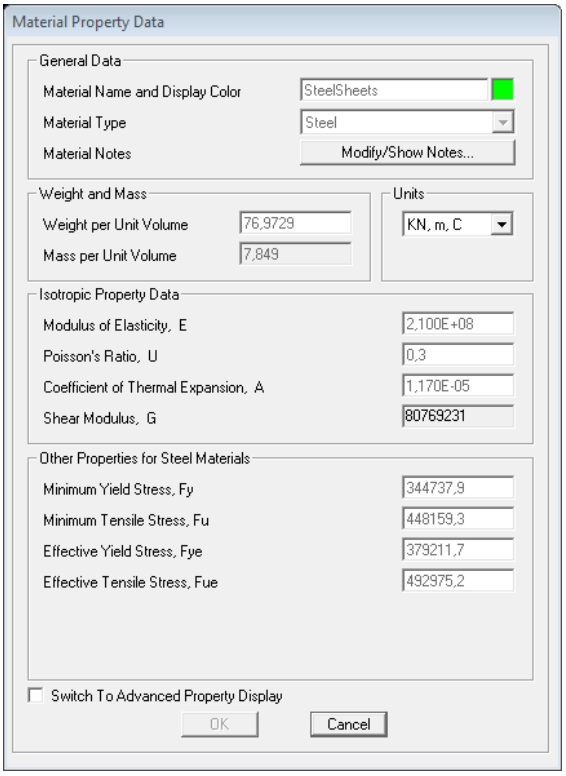

Figure 6-18. Material properties data.

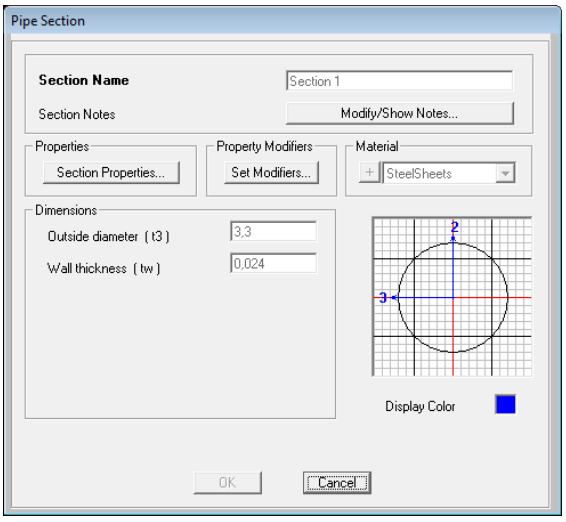

Figure 6-20. Cross section data

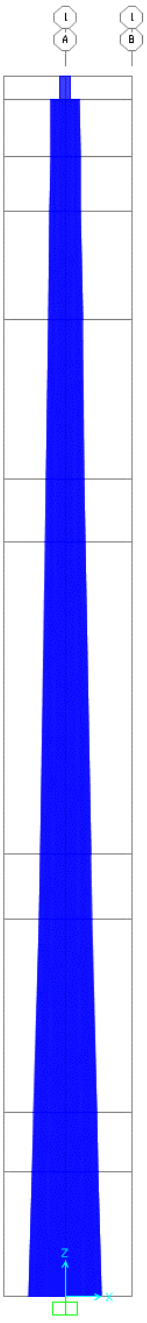

Figure 6-19. Tower elevation

6.3.2 Response History Analysis

Time history case was created using acceleration data exported from Matlab as seen in Figure 6-21. The Time history load case, see Figure 6-22, defines the acceleration data as a load. Table 6-11 summarizes the results gathered from three location in question.

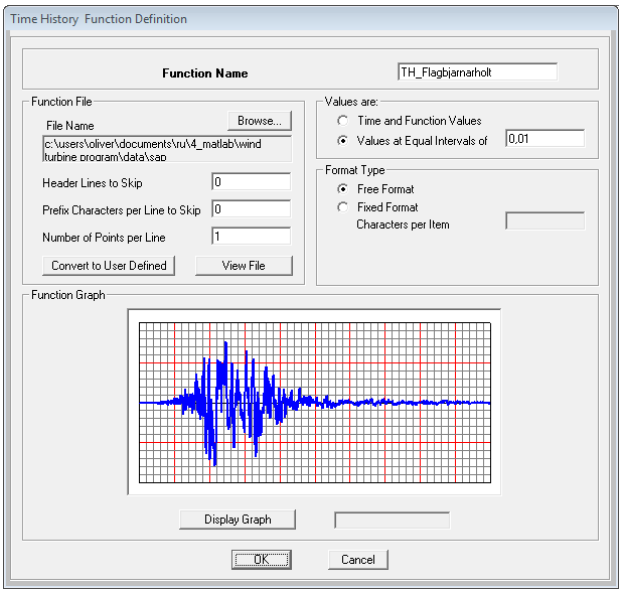

Figure 6-21. Time history definition, acceleration data from Flagbjarnarholti.

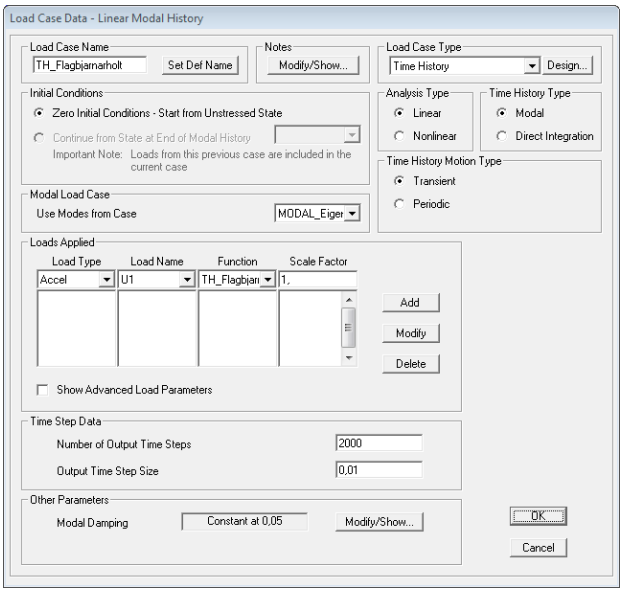

Figure 6-22. Load case definition from Time History definintion

Table 6-11. Summary of results from Time History anlysis made in SAP 2000

Station	D_{peak}	V_{bpeak}	M_{bpeak}	σ_{max}
	$[m]$	$[kN]$	$[MNm]$	$[MPa]$
Flagbjarnarholt	0,32	248	8,2	78
Þjórsárbrú	0,58	361	13,7	136
Hveragerði	0,30	218	7,3	60

6.3.3 Response Spectrum Analysis

Response Spectrum case was created using Periods and Response spectrum data exported from Matlab as seen in Figure 6-23. The Response Spectrum load case, see Figure 6-24, defines the acceleration data as a load. Table 6-12 summarizes the results gathered from three location in question.

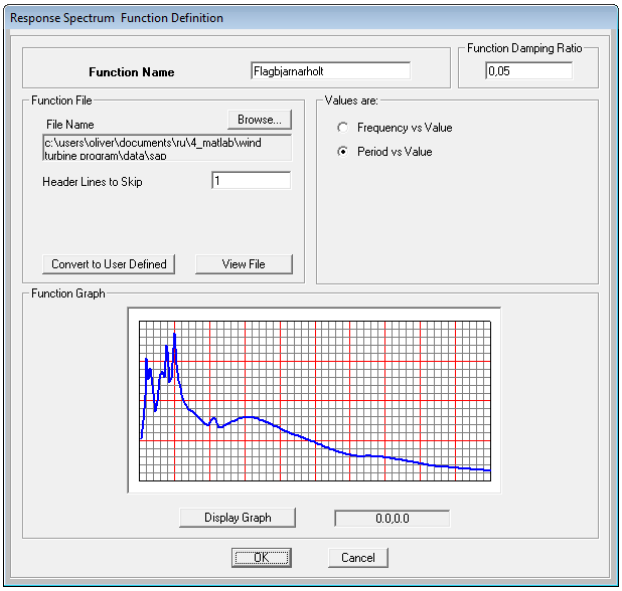

Figure 6-23. Response Spectrum definition, acceleration data from Flagbjarnarholti.

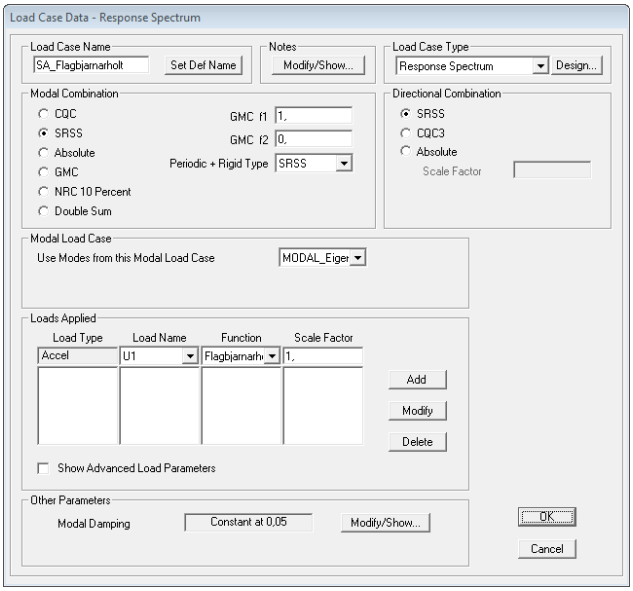

Figure 6-24. Load case definition from Response Spectrum definintion

Table 6-12. Summary of results from Response spectrum anlysis made in SAP 2000

Station	D_{peak}	$V_{b_{peak}}$	$M_{b_{peak}}$	σ_{max}
	$[m]$	$[kN]$	$[MNm]$	$[MPa]$
Flagbjarnarholt	0,321	175	6,9	65
Þjórsárbrú	0,584	314	12,7	117
Hveragerði	0,303	178	6,6	60

7 Concluding Remarks & Further Research

7.1 Concluding Remarks

The turbine is modelled using FEM techniques in SAP2000 and Matlab. The analysis workflow includes the selection of seismic data, modal analysis, response history analysis and response spectrum analysis.

Table 7-1. Summarizes the lateral mode shapes for the 3 and 10 element model and SAP model and it shows that they are relatively the same for all models, especially in Mode 1. The 900 kW reference turbine, discussed in section 2.3, has a slight higher natural frequency in the first mode but the second mode frequency is about the same as for the Enercon wind turbine studied herein.

Table 7-1. Summary of Mode 1 to Mode 3 for all models

Lateral Modes	**3 Element model**	**10 Element model**	**3D SAP model**	**900 kW Ref. Model**
	Frequency (Hz)	Frequency (Hz)	Frequency (Hz)	Frequency (Hz)
1	0,48	0,48	0,47	0.56
2	3,63	3,90	3,72	3,96
3	10,77	10,56	10,37	8,86

Response History and Spectrum analysis

Table 7-2, summarizes the top displacements and base reactions of all models resulting from Time History analysis and Response Spectrum Analysis, in Matlab and SAP2000.

Comparison of the base shear evaluated by the SAP2000 program using RHA analysis and the Matlab analysis for the recordings at Þjórsárbrú, on June 21, 2000, shows only a 11,3% difference compared to the 3 element model and 8,6% difference compared to the 10 element model. These differences are less when we compare the SAP2000 modal parameters that were used for repsonse analyses in Matlab to the pure Matlab models using 3 and 10 element respectivly. In this case, the difference in the evaluated base shear is only 2.7% and 0.2% respectively. Comparing the base moment evaluated by the SAP2000 model and the 3 element Matlab model is similarly 11.6% and 4.2% compared to the 10 element model. Looking at the Response Spectrum analysis, analogous results are gathered, as seen in Table 7-2.

Table 7-2. Summary of reaction forces and displacements for all analysis methods.

Type of analysis	**Flagbjarnarholt***			**Þjórsárbrú**			**Hveragerði**		
	17.06.2000			**21.06.2000**			**29.05.2008**		
	D	V	M	D	V	M	D	V	M
	$[m]$	$[kN]$	$[MNm]$	$[m]$	$[kN]$	$[MNm]$	$[m]$	$[kN]$	$[MNm]$
3 Element model									
TH analysis with Matlab	-	-	-	0,571	407	15,5	0,300	238	7,2
SA analysis with Matlab	-	-	-	0,534	333	13,2	0,300	181	6,9
10 Element model									
TH analysis with Matlab	0,322	245	8,2	0,574	395	14,3	0,303	268	8,0
SA analysis with Matlab	0,320	199	7,4	0,572	334	13,1	0,303	210	7,0
SAP model									
TH analysis with Matlab	0,320	245	8,0	0,583	396	14,4	0,301	238	7,3
SA analysis with Matlab	0,317	175	6,9	0,583	316	12,6	0,301	196	6,5
SAP model									
TH analysis with SAP2000	0,320	248	8,2	0,58	361	13,7	0,30	218	7,3
SA analysis with SAP2000	0,321	175	6,9	0,584	314	12,7	0,303	178	6,6

**The seismic activity at Kaldárholt gave the most reaction forces when analysed with a 3 element model, Flagbjarnarholt followed with a 450 kNm less base moment.*

The main difference between the SAP model analysed in Matlab and the 10 element model is related to the fact that the analysis made in SAP has three degrees of freedom ($u_x, u_y \; and \; r_y$) while the Matlab model after condensation has only one (u_x). Removing the rotational stiffness on Matlab indicates that the rotational stiffness reduces the effect of base reaction, as seen in the results in Table 7-2.

The Riso standard recommendation, to only consider a single mode shape to estimate the seismic load, is unsafe. Higher modes should be considered especially considering the effect on shear force distribution along the tower and potential risk from vertical loads in the near-field region. IEC and GL on the other hand do consider higher modes, or at least three modes in GL and consecutive modes with a total modal mass of 85% of the total mass in IEC guideline.

Neither Riso nor GL provide guidance regarding the level of viscous damping, leaving the designer to choose a suitable level, usually 5%, from other codes such as the Eurocode or the international building code (ICC, 2006). IEC suggested a 1% damping to establish the design response acceleration based on the first tower mode, but as seen in section 2.3, Prowell et al. (2010) found the first tower mode to have a damping of somewhere between 3 to 4%, then reducing at higher modes as seen in Table 2-1 (Prowell I. , Elgamal, Romanowitz, Duggan, & Jonkman, 2010).

The study done in Oak Creek showed a 12,5 MNm base moment for an operating scenario with aerodynamics and earthquake loading as well as for the independent parked turbine with earthquake loading only. Considering the results from operating scenario with only the aerodynamic load, a 10,1 MNm base moment was measured, and using the superimposed method for seismic loads and

normal-external loads would result in a moment demand of 22,6 MNm, in comparison with the 12,5 MNm.

Comparing the maximum demand from this study of 15,5 MNm to the results of Oak Creek's study shows that such a difference in an estimate of demand would likely have design implications on the turbine, which raises questions about the accuracy and level of conservatism when conducting independent simulations.

7.2 Further Research

Additional research to further investigate the effects of seismic loads for wind turbines is clearly needed to gather a more reliable information on the seismic risk and seismic behaviour of wind turbines.

Data from the continuous monitoring of operational turbines and their surroundings in seismically active regions is needed in order to gain access to data with better characteristics, since data from an instrumented turbine subjected to an actual earthquake is extremely valuable.

This type of monitoring also provides information that can help determine the appropriate level of damping, since the damping should not be considered as a single value but rather evaluated at each mode of vibration.

Further analysis are required that evaluates the 3D structural response based on simultaneous application of all three orthogonal ground acceleration components to understand better the true effects of near-field excitation.

Further analysis should consider possible non-linear response of wind turbines as well as soil structure interaction effects.

8 Bibliography

Ambraseys, N. N., & Sigbjörnsson, R. (2000). Re-appraisal of the seismicity of Iceland. (E. E. Centre, Ed.) *Polytechnica*, 196.

Ambraseys, N., Smit, P., Douglas, J., Margaris, B., Sigbjörnsson, R., Ólafsson, S., . . . Costa, G. (2004). Internet-site for European strong-motion data. *Bollettino di Geofisica Teorica ed Applicata, 45(3):*, 113-129.

Ákason, J., Ólafsson, S., & Sigbjörnsson, R. (2006a). Perception and observation of residential safety during earthquake exposure: a case study. *Saf Sci, 26(5)*, 919-933.

Ákason, J., Ólafsson, S., & Sigbjörnsson, R. (2006b). Phases of earthquake experience: a case study of the June 2000 South Iceland earthquake. *Risk Anal, 26(5)*, 1235-1246.

Bazeos, N., Hatzigeorgiou, G. D., Hondros, I. D., Karamaneas, H., Karabalis, D. L., & Beskos, D. E. (2002). Static, seismic and stability analyses of a prototype wind turbine steel tower. *Engineering Structures, 24(8)*, 1015-1025.

Bolt, B. A. (1999). *Earthquakes. 4th Edition.* New York: W.H. Freeman and Company.

Bommer, J. J. (2001). *Basics of Seismology and Seismic Hazard Assessment.* Pavia: ROSE School.

Bommer, J. J., Douglas, J., & Strasser, F. O. (2003). Style-of-Faulting in Ground-Motion Prediction Equations. *Bulletin of Earthquake Engineering*, 171 - 203.

Bossanyi, E. A. (2003). *Bladed for Windows User MAnual.* Bristol: Garrad Hassan and Partners.

Burton, T., Sharpe, D., Jenkins, N., & Bossanyi, E. (2001). *Wind Energy - Handbook.* West Sussex: John Wiley & Sons, LTD,.

Chopra, A. K. (2007). *Dynamics of structure: Theory and applications to earthquake engineering* (Third edition ed.). New Jersey: Pearson Prentice Hall.

CSA. (2008). *Wind Turbines - Part 1: Design requirements. Standard CAN/CSA C61400-1:08.* Toronto, Ont.: Canadian Standards Association.

Elnashai, A. S., & Sarno, L. D. (2008). *Fundamentals of earthquake engineering.* Chichester, West Sussex: John Wiley & Sons.

Germanischer Lloyd. (2003). *Guideline for the Certification of Wind Turbines.* Hamburg: Germanischer Lloyd.

GL. (2003). *Guidelines for the Certification of Wind Turbines.* Hamburg, Germany: Germanischer Lloyd.

Global CMT Catalog. (2007, June 22). *Homepage: Global CMT Catalog Search*. Retrieved from Global CMT Catalog Search: http://www.globalcmt.org/CMTsearch.html

Guðmundsson, Á. (2000). Dynamics of volcanic systems in Iceland: Example of Tectonism and Volcanism at Juxtaposed Hot Spot and Mid-Ocean Ridge Systems. *Annual Review of Earth and Planetary Sciences*, 107 - 140.

Halldórsson, B., Ólafsson, S., & Sigbjörnsson, R. (2007). A fast and efficient simulation of the far-field and nearfault earthquake ground motions associated with the June 17 and 21, 2000, earthquakes in South Iceland. *J Earthq Eng, 11:*, 343-370.

ICC. (2006). *International Building Code 2006.* Illinois: International Code Council.

IEC. (2005). *Wind Turbines - Part 1: Design requirements. 3rd ed. Standard IEC 61400-1:2005-08.* Geneva, Switzerland: International Electrotechnical Commission.

James, P., & Thorpe, N. (1994). *Ancient Inventions.* New York: Ballantine Books.

Jonkman, J. M., & Buhl Jr, M. L. (2005). *FAST user¨s guide.* Colorado: National Renewable Energy Laboratory.

Jonkman, J., Butterfield, S., Musial, S., & Scott, G. (2009). *Definition of a 5-MW Reference Wind Turbine for Offshore System development.* National Renewable Energy Laboratory.

Landsvirkjun. (2013, November 15). *Vindmyllur: Landsvirkjun*. Retrieved from Landsvirkjun.is: http://www.landsvirkjun.is/Rannsoknirogthroun/Throunarverkefni/Vindmyllur/

Larsen, T. J. (2009). *How 2HAWC2, the user's manual.* Roskilde: Risø National Laboratory Technical Inivesity of Denmark.

Lavassas, I., Nikolaidis, G., Zervas, P., Efthimiou, E., Doudoumis, I. N., & Baniotopoulos, C. C. (2003). Analysis and design of the prototype of a steel 1-MW wind turbine tower. *Engineering Structures, 25(8)*, 1097-1106.

Nawri, N., Petersen, G. N., Björnsson, H., Hahmann, A. N., Jónasson, K., Hasager, C. B., & Clausen, N.-E. (2014). The wind energy potential of Iceland. *ScienceDIrect*, 290-299.

Orkustofnun. (2013). *Orkutölur 2013.* Reykjavík: Orkustofnun. Retrieved from http://os.is/gogn/os-onnur-rit/orkutolur_2013-islenska.pdf

Prowell, I., Elgamal, A., & Jinchi, L. (2010). Modeling the Influence of Soil Structure Interaction on the Seismic Response of a 5 MW Wind Turbine. *5th International Conference on Recent Advances in Geotechnical Earthquake Engineering and Soil Dynamics.* San Diego.

Prowell, I., Elgamal, A., & Jonkman, J. (2010). Seismic Response of a 5 MW Wind Turbine; The shakeout Scenario.

Prowell, I., Elgamal, A., Romanowitz, H., Duggan, J. E., & Jonkman, J. (2010). *Earthquake Response Modeling for a Parked and Operating Megawatt-Scale Wind Turbine.* Colorado: National Renewable Energy Laboratory.

Richter, C. F. (1958). *Elementary Seismology.* San Francisco: W.H. Freeman and Company.

Risø. (2001). *Guidelines for Design of Wind Turbines.* Copenahgen, Denmark: Wind Energy Department of Risø National Laboratory and Det Norske Veritas.

Scholz, C. H. (1990). *The Mechanics of Earthquakes and Faulting.* Cambridge: Cambridge Press.

Sigbjörnsson, R., & Ólafsson, S. (2004). On the South Iceland earthquake in June 2000. *Bollettino di Geofisica Teorica ed Applicata, 45(3)*, 131-152.

Sigbjörnsson, R., & Ólafsson, S. (2004). On the South Iceland earthquakes in June 2000: strong-motion effects and. *Bollettino di Geofisica Teorica ed Applicata, 45*, 131-152.

Sigbjörnsson, R., Ólafsson, S., & Snæbjörnsson, J. T. (2007). Macroseismic effects related to strong ground motion: a study of the South Iceland earthquakes in June 2000. *Bull Earthquake Eng , 5*, 591-608.

Sigbjörnsson, R., Snæbjörnsson, J. T., Higgins, S. M., Halldórsson, B., & Ólafsson, S. (2009). A note on the Mw 6.3 earthquake in Iceland on 29 May. *Bull Earthquake Eng, 7:*, 113-126.

Sólnes, J., Sigmundsson, F., & Bessason, F. (Eds.). (2013). *Náttúruvá á Íslandi: Eldgos og Jarðskjálftar*. Reykjavík: Viðlagatrygging Íslands/Háskólaútgáfan.

Srbulov, M. (2010). Ground vibration engineering Simpified Analysis with Case studies and Examples,. (Springer, Ed.) *Geological and Earthquake Engineering, volume 12(17) of Geotechnical*.

Wiser, M., & Bolinger, M. (2013). *2012 Wind technologies Market Report.* Washington, DC: U.S. Department of Energy.

Appendix A

Input data used in Matlab Response History Analysis and Response Spectrum Analysis. These files can be abdapted to other kinds of wind turbines.

```
%-------------------------------------------------------------
%--Tower input file-----------------------------------------
%Description:
%--SIMULATION CONTROL ---------------------------------------
%NE - Number of elements
3
%Nmod - Number of modes
3
%G - Gravitational acceleration (m/s^2)
9.81
%Damping
0.01 0.05
%Modulus     - Modulus of elasticity in N/m2
210e+09
%Hro         - Steel density
7850
%-------------------------------------------------------------
%x      %W          %Ix
17.03   2.4995e+04  0.1877
17.0    1.4896e+04  0.0610
19.92   1.2199e+04  0.0235
%-------------------------------------------------------------
37000       %W_top - Nacelle and rotor weight


%-------------------------------------------------------------
%--Tower input file-----------------------------------------
%Description:
%--SIMULATION CONTROL ---------------------------------------
%NE - Number of elements
10
%Nmod - Number of modes
10
%G - Gravitational acceleration (m/s^2)
9.81
%Damping
0.01 0.05
%Modulus     - Modulus of elasticity in N/m2
210e+09
%Hro         - Steel density
7850
%-------------------------------------------------------------
%x      %W      %Ix
5.61    10389   0.2887
2.7     3978    0.1947
8.72    11024   0.1271
2.92    3101    0.0857
14.08   12723   0.0553
2.82    1991    0.0319
7.2     4286    0.0225
4.87    2241    0.0171
2.47    1225    0.0164
```

```
2.56    1391    0.0153
37000       %W_top       - Nacelle and rotor weight
```

Input data from SAP 2000 used in Matlab Response History Analysis and Response Spectrum Analysis

Table 8-1. Element height and weight

Joint	H	U1
Text	m	KN-s2/m
1	0	5280
2	5,61	7070
3	2,7	7140
4	8,72	6450
5	2,92	7400
6	14,08	6420
7	2,82	3040
8	7,2	3080
9	4,87	1630
10	2,47	1260
11	2,56	670
23	1,05	37000

Table 8-2. Tower Mode shapes

1	2	3	4	5	6	7	8	9	10
Unitless	Unitless	Unitless	Unitless	Unitless	Unitless	Unitless	Unitless	Unitless	Unitless
0,000	0,000	0,000	0,000	0,000	0,000	0,000	0,000	0,000	0,000
-0,001	0,010	-0,035	0,000	0,032	-0,200	0,036	0,000	-0,080	-0,076
-0,002	0,021	-0,069	0,000	0,058	-0,279	0,043	0,000	-0,034	-0,014
-0,009	0,088	-0,205	0,000	0,107	-0,014	-0,032	0,000	0,209	0,211
-0,013	0,118	-0,228	0,000	0,081	0,128	-0,019	0,000	-0,130	-0,168
-0,049	0,252	0,010	0,000	-0,206	-0,004	0,113	0,000	-0,119	0,142
-0,060	0,259	0,093	0,000	-0,134	-0,070	-0,107	0,000	0,342	-0,311
-0,092	0,213	0,239	0,000	0,273	-0,023	-0,318	0,000	-0,146	0,095
-0,119	0,122	0,198	0,000	0,348	0,089	0,403	0,000	0,047	-0,017
-0,133	0,059	0,123	0,000	0,242	0,082	0,446	0,000	0,132	-0,092
-0,148	-0,012	0,023	0,000	0,059	0,024	0,135	0,000	0,045	-0,032
-0,155	-0,041	-0,020	0,000	-0,021	-0,004	-0,016	0,000	-0,003	0,002

Table 8-3. Participation factor in x and z direction

StepNum	UX	SumUX	UZ	SumUZ	RY	SumRY
Unitless	Unitless	Unitless	Unitless	Unitless	Unitless	Unitless
1	0,63	0,63	0,00	0,00	0,96	0,96
2	0,15	0,78	0,00	0,00	0,03	0,99
3	0,10	0,88	0,00	0,00	0,01	1,00
4	0,00	0,88	0,73	0,73	0,00	1,00
5	0,02	0,90	0,00	0,73	0,00	1,00
6	0,09	0,99	0,00	0,73	0,00	1,00
7	0,00	0,99	0,00	0,73	0,00	1,00
8	0,00	0,99	0,16	0,89	0,00	1,00
9	0,00	0,99	0,00	0,89	0,00	1,00
10	0,00	0,99	0,00	0,89	0,00	1,00
11	0,00	0,99	0,05	0,94	0,00	1,00

Table 8-4. Natural frequencies of the tower.

StepNum	Period	Frequency	CircFreq	Eigenvalue
Unitless	Sec	Cyc/sec	rad/sec	rad2/sec2
1	2,13	0,47	2,95	8,67
2	0,27	3,72	23,37	546,11
3	0,10	10,37	65,17	4246,50
4	0,07	14,63	91,93	8451,80
5	0,05	18,40	115,62	13369,00
6	0,03	38,19	239,93	57567,00
7	0,02	48,25	303,15	91899,00
8	0,02	53,06	333,41	111160,00
9	0,01	78,97	496,17	246180,00
10	0,01	88,43	555,63	308720,00
11	0,01	90,61	569,30	324110,00

Appendix B

Run_External.m

```
clc
clear all
close all
global NE K_sc g Ndivide am Ndir H Umax Nmod wr_sum mm hn_s Mn_s Dt Vt...
       Mt maxMb_SA maxMb_TH H_tot dm w2 Data pf Mb Vb aglob dglob vglob...
       dataArray ers_T  name fault Dt_t Vb_t Mb_t st_name st_fault...
       acc_or corData ers tm a PGA %#ok<NUSED>
input_file = 'Enercon_900kW_10el.txt';
Import_Data
```

Lumped system mass matrix

```
M_dist = [5/8 3/8];     % Mass distribution factor between point 1 and 2.
W_dist = zeros(2,NE + 1);
j = 0;
for idist = 1:2
        W_dist(idist,idist:NE + j) = W(1:end);
        j = j + 1;
end
% Diagonal mass matrix
M_lm = diag(M_dist*W_dist);
% Boundary conditions
M_lm = M_lm(2:end,2:end);
% Add the mass of rotor and Nacelle
M_lm(end,end) = M_lm(end,end) + W_top;
```

Element stiffness

```
for i = 1:NE
    L = H_el(i);
    K_vec(:,:,i) = E*Ix(i)/L^3*...
                   [12    6*L    -12    6*L;
                    6*L   4*L^2  -6*L   2*L^2;
                   -12   -6*L     12   -6*L;
                    6*L   2*L^2  -6*L   4*L^2];
end
```

Stiffness matrix

```
K_mat = zeros(2*NE+2);
K_tmp = zeros(2*NE+2);

j=0;
for i=1:2:2*NE

    j=j+1;
    K_tmp(i:3 + i,i:3 + i,j) = K_vec(:,:,j);

end

K_mat = sum(K_tmp,3);

% Boundary conditions: fixed at base
K_mat = K_mat(3:end,3:end);
```

Static condensation to remove rotational DOF

```
Ktt = K_mat(1:2:end,1:2:end);
K0t = K_mat(2:2:end,1:2:end);
Kt0 = K_mat(1:2:end,2:2:end);
K00 = K_mat(2:2:end,2:2:end);
K_sc = Ktt-K0t'*inv(K00)*K0t;
K_sc_diag = diag(K_sc);
```

Free undamped vibration

```
[fi,w2] = eig(K_sc, M_lm);
[w2,I] = sort(diag(w2),1,'ascend');
fi = fi(:,I);
wn = sqrt(w2);        % Computing the natural frequency in rad/sek.
fn = wn/(2*pi);       % Computing the natural frequency in Hz.
Tn = 1./fn;           % Computing the natural period.
```

Selecting Seismic data

```
SeismicData;
```

Modal anlysis

```
[sn, Um, Vm, Mm] = ModalAnalysis(fi, M_lm, H_el);
```

Response History Analysis

```
[U_TH, V_TH, OTM_TH, Vstep_TH, Hstep_TH] = Response_History_Analysis(H_el_sum, Um,
Vm, Mm, xi, Tn, fi);
```

Response Spectrum Analysis

```
[T, as_vec, ds_Tn, vs_Tn, as_Tn, U_SA, V_SA, OTM_SA, Vstep_SA, Hstep_SA] =
Response_Spectrum_Analysis(H_el_sum, Um, Vm, Mm, Tn, xi);
[MaxData, Location] = MaximumValue(U_TH, U_SA, V_TH, V_SA, OTM_TH, OTM_SA,
maxMb_TH, maxMb_SA);
```

Maximum reaction values

```
[MaxData, Location] = MaximumValue(U_TH, U_SA, V_TH, V_SA, OTM_TH, OTM_SA,
maxMb_TH, maxMb_SA);
```

Plot

```
Plot(H_el_sum, Hstep_TH, Vstep_TH, Vstep_SA, U_TH, U_SA, V_TH, V_SA, OTM_TH,
OTM_SA);                              % Plot Data
```

Run_SAP.m

```
clear all
close all
clc
%global H_tot H_el_sum M_lm NE Nmod g pf Ndivide Vstep Hstep a tm PGA st_name
st_fault Mb_x Mb_y
global NE K_sc H_el PGA g Ndivide am Ndir Nmod mm hn_s Mn_s H_tot maxMb_SA
maxMb_TH...
       Data pf dataArray ers_T st_name acc_or corData ers %#ok<NUSED>
% [fileName_SAP, pathName, filterindex] = uigetfile( ...
% {  '*.xlsx','xlsx-files (*.xlsx)'; ...
%    '*.*',  'All Files (*.*)'}, ...
%    'Pick a file');
fileName_SAP = 'Data_Summary2.xlsx';
g = 9.81;
Nmod = 11;
xi = 0.05; %[0.01 0.02 0.05];
```

Read data from SAP

```
% Assembled Joint Masses
[~,~,RAW] = xlsread(fileName_SAP,'Joint placements','C4:C15');
M_lm = diag(cell2mat(RAW(2:end))); %kg
% Joint coordinates
[~,~,RAW] = xlsread(fileName_SAP,'Joint placements','B4:B15');
H_el = cell2mat(RAW(2:end))';
H_el_sum = cumsum(H_el);
H_tot = H_el_sum(end);
% Modal displacements
[~,~,RAW] = xlsread(fileName_SAP,'Mode shapes','B4:L15');
fi = cell2mat(RAW(2:end,:));
% Modal Participation Factorsfi
[~,~,RAW] = xlsread(fileName_SAP,'Modal Participation Factors','F4:F14');
k_mod = cell2mat(RAW);
% Modal Participation Mass Ratio
[~,~,RAW] = xlsread(fileName_SAP,'Modal Participating Mass Ratios','B4:B14');
pf_SAP = cell2mat(RAW(2:end));
% Modal Periods and Frequencies
[NUM,TXT,RAW] = xlsread(fileName_SAP,'Modal Periods And Frequencies','B4:E15');
Tn = cell2mat(RAW(:,1));
fn = cell2mat(RAW(:,2));
wn = cell2mat(RAW(:,3));
w2 = cell2mat(RAW(:,4));
NE = 11;
```

Selecting Seismic data

```
SeismicData;
```

Modal anlysi

```
[sn, Um, Vm, Mm] = ModalAnalysis(fi, M_lm, H_el);
```

Response History Analysis

```
[U_TH, V_TH, OTM_TH, Vstep_TH, Hstep_TH] = Response_History_Analysis(H_el_sum, Um,
Vm, Mm, xi, Tn, fi);
```

Response Spectrum Analysis

```
[T, as_vec, ds_Tn, vs_Tn, as_Tn, U_SA, V_SA, OTM_SA, Vstep_SA, Hstep_SA] =
Response_Spectrum_Analysis(H_el_sum, Um, Vm, Mm, Tn, xi);
```

Maximum reaction values

```
[MaxData, Location] = MaximumValue(U_TH, U_SA, V_TH, V_SA, OTM_TH, OTM_SA,
maxMb_TH, maxMb_SA);
```

Plot

```
Plot(H_el_sum, Hstep_TH, Vstep_TH, Vstep_SA, U_TH, U_SA, V_TH, V_SA, OTM_TH,
OTM_SA);                              % Plot Data
```

SeismicData.m

```
function SeismicData
global pathName fileName csvData corData Ndir acc_or tme_or Ndata Ndivide ns dt tm
a PGA
```

Select Seismic data

```
[fileName, pathName] = uigetfile( ...
{  '*.*',  'All Files (*.*)';...
   '*.cor','COR-files (*.cor)';...
   '*.csv','CSV-files (*.csv)'},...
   'Pick a file', ...
   'MultiSelect', 'on');
if iscell(fileName)
    Ndata = length(fileName) - 1;
    Ndivide = floor(Ndata/2);
    fileName = sort(fileName);
    corData = reshape(fileName(1:end-1),2,Ndivide);
    csvData = fileName(end);
    Ndir = 2;
elseif fileName ~= 0
    Ndata = 1;
else
    Ndata = 0;
end
Location(pathName, csvData, corData)
```

Cut off data

```
noise = 0.5;                                % Length of noise section
duration = 20;                              % Duration of history accel. in sek
acc_or = cell(1,Ndivide);
tme_or = cell(1,Ndivide);
a = cell(1,Ndivide);
tm = cell(1,Ndivide);
j = 0;
k = 0;
for i = 1:Ndata
    j = j + 1;
    [~,tme,acc,~,~]=Cor_In(pathName,corData{i});
    dt = tme(2)-tme(1);                      % Time step
    Nstep = floor(noise/dt);                 % Number of steps in noise
    Nduration = floor(duration/dt) - 1;      % Number of steps in TH
    [~, nx] = max(abs(acc));                % Locating PGA
    Nmax = max(abs(acc(1:Nstep)));           % Maximum acceleration in noise
    Nstart = abs(find(abs(acc(1:nx)) > 3*Nmax,1,'first') - 200);  % Locating
starting point
    Nfinish = Nstart + Nduration;
    temp_acc_or(:,j) = acc';
    temp_tme_or(:,j) = tme';
    temp_a(:,j) = acc(Nstart:Nfinish)';
    temp_tm(:,j) = tme(Nstart:Nfinish)';
    if j == 2
        k = k + 1;
        acc_or{k} = temp_acc_or;
        tme_or{k} = temp_tme_or;
        a{k} = temp_a;
        tm{k} = temp_tm;
        PGA{k} = max(a{k});
        clear temp_a temp_tm temp_acc_or temp_tme_or
        j = 0;
        continue
    end
end
ns = Nfinish - Nstart + 1;
end
```

Location.m

```
function Location(pathName, csvData, corData)
global Ndivide st_name st_fault st_epicentre dataArray Data name fault
Loc = cell(1,Ndivide);
```

Initialize variables.

```
clc
Input = fullfile(pathName,csvData{1});
delimiter = ';';
```

Read columns of data as strings:

```
formatSpec =
'%s%s%s%s%s%s%s%s%s%s%s%s%s%s%s%s%s%s%s%s%s%s%s%s%s%s%s%s%s%s%s%s%s%s%s%s%s%s%s%s%s
%s%s%s%s%s%s%s%s%s%s%[^\n\r]';
```

Open the text file.

```
fileID = fopen(Input,'r');
dataArray = textscan(fileID, formatSpec, 'Delimiter', delimiter,...
                        'headerlines',2,'ReturnOnError', false);
```

Close the text file.

```
fclose(fileID);
switch csvData{1}
    case 'param15636.csv'
        Data = cellfun(@(x) x(3:6), corData(1:2:end), 'UniformOutput', false);
    case 'param15752.csv'
        Data = cellfun(@(x) x(3:6), corData(1:2:end), 'UniformOutput', false);
    Otherwise
        Data = cellfun(@(x) x(2:6), corData(1:2:end), 'UniformOutput', false);
end
for i = 1:Ndivide
Loc{i} = find(ismember(dataArray{1},Data{i}));
st_name{1}(i) = dataArray{21}(Loc{i})';
st_epicentre{1}(i) = dataArray{36}(Loc{i})';
st_fault{1}(i) = dataArray{37}(Loc{i})';
end
end
```

ModalAnalysis.m

```
function [sn, Um, Vm, Mm] = ModalAnalysis(fi, M_lm, H_el)
global NE Nmod hn_s Mn_s pf H wr_sum w2 tm a PGA %#ok<NUSED>
R = ones(NE,1);                 % Influence vector (Iota in Chopra)
Mn = diag(fi'*M_lm*fi);           % Generalized modal mass, mode n
Ln_h = fi'*M_lm*R;                %
Ln_theta = fi'*M_lm*H_el';        %
pf = Ln_h./Mn;                    % Participation factor
hn_s = Ln_theta./Ln_h;            % Effective modal height, mode n
Mn_s = pf.*Ln_h;                  % Effective modal mass, mode n
wr = 100*Mn_s/sum(diag(M_lm));    % Percentage of active mass
wr_sum = cumsum(wr);              % Cumulative percentage of active mass
sn = M_lm*fi*diag(pf);             % Modal inertia force distributions
Um = fi*diag(pf);
Vm = flipud(cumsum(flipud(sn)));   % Modal static response Vi
H = zeros(NE);                    % Moment arm matrix
for iel = 1:NE
    H(iel,iel:NE) = cumsum(H_el(iel:end));
end
Mm = H*sn;                         % Modal static moment Mi
end
```

Response_History_Analysis.m

```
function [U_TH, V_TH, OTM_TH, Vstep_TH, Hstep_TH] =
Response_History_Analysis(H_el_sum, Um, Vm, Mm, xi, Tn, fi)
global Ndamp Ndivide Ndir Umax Nmod NE ns dt Mt Vt Dt maxMb_TH...
       Dt_t Vb_t Mb_t Mb_x Mb_y Vb_x Vb_y am dm Mb Vb aglob dglob vglob tm a PGA
%#ok<NUSED>
```

Shear Forces and Overturning Moment

```
Ndamp = length(xi);
V = zeros(NE,Ndir,Ndamp);
OTM = zeros(NE,Ndir,Ndamp);
for istation = 1:Ndivide
    for idamp = 1:Ndamp
        for idir = 1:Ndir
            dm = zeros(ns,Nmod);
            vm = zeros(ns,Nmod);
            am = zeros(ns,Nmod);
            for iel = 1:Nmod
                Ti = Tn(iel);
                ag_t = a{istation}(:,idir);
                [d, v, ar] = NewmarkL(Ti,xi(idamp),ag_t,dt);
                dm(:,iel) = d;            % Modal displacement
                vm(:,iel) = v;            % Modal velocity
                am(:,iel) = ar + ag_t;    % Modal acceleration
            end
            % Element displacement
            Dt{istation}(:,:,idir,idamp) = dm*Um';
            U_TH(:,idir,idamp,istation) = flipud(max(abs(dm*Um'))');
            % Element shear
            Vt{istation}(:,:,idir,idamp) = am*Vm';
            V_TH(:,idir,idamp,istation) = flipud(max(abs(am*Vm'))')/(1e+03);   %
Story shear in kN
            for i = 1:2
                Vstep_TH(i:2:2*NE,idir,idamp,istation) =
V_TH(:,idir,idamp,istation)';
                Hstep_TH(i:2:2*NE) = H_el_sum(1,:);
            end
            % Element overturning moment
            Mt{istation}(:,:,idir,idamp) = am*Mm';
            OTM_TH(:,idir,idamp,istation) = flipud(max(abs(am*Mm'))')/(1e+06);   %
Story moment kNm
            % Time series
            dgl = fi*dm';     % global displacement
            vgl = fi*vm';     % global velocity
            agl = fi*am';     % global acceleration
            dglob(:,idir,idamp,istation) = dgl(3,:)';     % global displacement
            vglob(:,idir,idamp,istation) = vgl(3,:)';     % global velocity
            aglob(:,idir,idamp,istation) = agl(3,:)';     % global acceleration
        end
    end
end
maxUt_TH = reshape(max(U_TH(:,1,:,:)) >= max(U_TH(:,2,:,:)),Ndivide,1);
maxVb_TH = reshape(max(V_TH(:,1,:,:)) <= max(V_TH(:,2,:,:)),Ndivide,1);
maxMb_TH = reshape(max(OTM_TH(:,1,:,:)) >= max(OTM_TH(:,2,:,:)),Ndivide,1);
```

```
end
```

Response_Spectrum_Analysis.m

```
function [T, as_vec, ds_Tn, vs_Tn, as_Tn, U_SA, V_SA, OTM_SA, Vstep_SA, Hstep_SA] =
Response_Spectrum_Analysis(H_el_sum, Um, Vm, Mm, Tn, xi)
global Ndivide Ndamp dt Ndir ers g Nmod NE tm a PGA maxMb_SA %#ok<NUSED>
T = linspace(0,4,200);                    % Period 0 - 4 sek
for iTn = 1:Nmod
    [~,Tn_pos(iTn)] = find(T >= Tn(iTn),1,'first');
end
Ndamp = length(xi);
Nt = length(T);
ds_vec = zeros(Nt,Ndir,Ndamp,Ndivide);
ds_Tn = zeros(Nmod,Ndir,Ndamp,Ndivide);
vs_vec = zeros(Nt,Ndir,Ndamp,Ndivide);
vs_Tn = zeros(Nmod,Ndir,Ndamp,Ndivide);
as_vec = zeros(Nt,Ndir,Ndamp,Ndivide);
as_Tn = zeros(Nmod,Ndir,Ndamp,Ndivide);
ers = zeros(Nt,2,Ndamp,Ndivide);
for istation = 1:Ndivide
    for idamp = 1:Ndamp
        for idir = 1:Ndir
            ag = a{istation}(:,idir);
            PGA_S = max(ag);
            [ers_T] = Eurospectrum(xi(idamp), T, PGA_S);          % Eurocode
spectra
            ers(:,:,idamp,istation) = ers_T;
            ds = zeros(Nt,1);
            vs = zeros(Nt,1);
            as = zeros(Nt,1);
            for iPeriod = 1:Nt
                Ti = T(iPeriod);
                [d, v, ar] = NewmarkL(Ti,xi(idamp),ag,dt);
                  ds(iPeriod,1) = max(abs(d));       % Spectral displacement
                  vs(iPeriod,1) = max(abs(v));       % Spectral velocity
                  as(iPeriod,1) = max(abs(ar + ag)); % Spectral acceleration
            end
            ds_vec(:,idir,idamp,istation) = ds;
            ds_Tn(:,idir,idamp,istation) = ds(Tn_pos);
            vs_vec(:,idir,idamp,istation) = vs;
            vs_Tn(:,idir,idamp,istation) = vs(Tn_pos);
            as_vec(:,idir,idamp,istation) = as;
            as_Tn(:,idir,idamp,istation) = as(Tn_pos);
            j = 0;
            for iel = NE:-1:1
                   j = j + 1;
                U_SA(iel,idir,idamp,istation) =
flipud(sqrt(sum((Um(j,:).*ds_Tn(:,idir,idamp,istation)').^2,2)));
                V_SA(iel,idir,idamp,istation) =
sqrt(sum((Vm(j,:).*as_Tn(:,idir,idamp,istation)').^2,2))/(1e+03);
                OTM_SA(iel,idir,idamp,istation) =
sqrt(sum((Mm(j,:).*as_Tn(:,idir,idamp,istation)').^2,2))/(1e+06);
            End
            for i = 1:2
                Vstep_SA(i:2:2*NE,idir,idamp,istation) =
V_SA(:,idir,idamp,istation)';
                Hstep_SA(i:2:2*NE) = H_el_sum(1,:);
```

```
            end
        end
    end
end
maxMb_SA = reshape(max(OTM_SA(:,1,:,:)) >= max(OTM_SA(:,2,:,:)),Ndivide,1);
end
```